

**FLUORESCENT HYDRAZINE-NAPHTHALIMIDE
ENCAPSULATED BY ETHYL CELLULOSE FOR
DETECTION OF LONG-CHAIN ALDEHYDES**



Mrs. Faiza Lawan Isah

จุฬาลงกรณ์มหาวิทยาลัย
CHULALONGKORN UNIVERSITY

**A Thesis Submitted in Partial Fulfillment of the Requirements
for the Degree of Master of Science in Chemistry
Department of Chemistry
FACULTY OF SCIENCE
Chulalongkorn University
Academic Year 2022
Copyright of Chulalongkorn University**

ฟลูออเรสเซนซ์ไอศราจีน-แนพทาลีไมด์ห่อหุ้มด้วยเอทิลเซลลูโลสสำหรับการตรวจวัดแอลดีไฮด์
สายยาว



วิทยานิพนธ์นี้เป็นส่วนหนึ่งของการศึกษาตามหลักสูตรปริญญาวิทยาศาสตรมหาบัณฑิต
สาขาวิชาเคมี ภาควิชาเคมี
คณะวิทยาศาสตร์ จุฬาลงกรณ์มหาวิทยาลัย
ปีการศึกษา 2565
ลิขสิทธิ์ของจุฬาลงกรณ์มหาวิทยาลัย

Thesis Title FLUORESCENT HYDRAZINE-
NAPHTHALIMIDE ENCAPSULATED BY
ETHYL CELLULOSE FOR DETECTION OF
LONG-CHAIN ALDEHYDES
By Mrs. Faiza Lawan Isah
Field of Study Chemistry
Thesis Advisor Associate Professor BOOSAYARAT
TOMAPATANAGET, Ph.D.

Accepted by the FACULTY OF SCIENCE, Chulalongkorn University
in Partial Fulfillment of the Requirement for the Master of Science

..... Dean of the FACULTY OF
SCIENCE
(Professor POLKIT SANGVANICH, Ph.D.)

THESIS COMMITTEE

..... Chairman
(Professor PATCHANITA THAMYONGKIT,
Ph.D.)

..... Thesis Advisor
(Associate Professor BOOSAYARAT
TOMAPATANAGET, Ph.D.)

..... Examiner
(Professor THAWATCHAI TUNTULANI, Ph.D.)

..... Examiner
(Associate Professor FUANGFA UNOB, Ph.D.)

..... External Examiner
(Associate Professor Thanthapatra Bunchuay, Ph.D.)

พายชา ลาวาน อิศข่า : ฟลูออเรสเซนต์ไฮดราซีน-แนพทาลิไมด์ห่อหุ้มด้วยเอทิลเซลลูโลสสำหรับการตรวจวัดแอลดีไฮด์สายยาว. (FLUORESCENT HYDRAZINE-NAPHTHALIMIDE ENCAPSULATED BY ETHYL CELLULOSE FOR DETECTION OF LONG-CHAIN ALDEHYDES) อ.ที่ปรึกษาหลัก :
รศ. ดร.บุษยรัตน์ ธรรมพัฒน์กิจ

โรคมะเร็งปอดเป็นหนึ่งในโรคสำคัญที่มีผู้เสียชีวิตจำนวนมากทั่วโลก สารอัลดีไฮด์ความเข้มข้นสูงที่พบในควันบุหรี่และไอเสียรถยนต์เป็นปัจจัยหนึ่งที่ทำให้เกิดโรคมะเร็งปอด เช่นเซอรันนาโนสำหรับการตรวจวัดอัลดีไฮด์สายยาวจึงได้รับความสนใจอย่างมาก วิธีการตรวจวัดอัลดีไฮด์แบบดั้งเดิมมีความซับซ้อนสูง ราคาแพง และใช้เวลานาน เพื่อกำจัดข้อเสียนี้จึงใช้ เทคนิคฟลูออเรสเซนต์ เป็นอีกทางเลือกหนึ่งในการระบุอัลดีไฮด์ได้อย่างรวดเร็ว ง่าย และราคาไม่แพง การใช้สารประกอบอัลดีไฮด์และอนุพันธ์ของสารประกอบอัลดีไฮด์เป็นตัวบ่งชี้ทางชีวภาพของมะเร็งปอด ทำให้สามารถวินิจฉัยและคาดว่าจะรักษาผู้ป่วยมะเร็งปอดได้ตั้งแต่ระยะเบื้องต้น ดังนั้นการพัฒนาเซ็นเซอร์นาโนที่มีประสิทธิภาพสำหรับการตรวจวัดอัลดีไฮด์สายยาวเป็นที่น่าสนใจอย่างมาก ในงานนี้ได้ใช้เทคนิคฟลูออเรสเซนต์เพื่อพัฒนาและเตรียมเซ็นเซอร์นาโนเรืองแสงที่ละลายน้ำได้โดยการห่อหุ้มสารสีย้อมแนพทาลิไมด์ด้วยเอทิลเซลลูโลสเพื่อสร้างเซ็นเซอร์ระดับนาโนที่มีประสิทธิภาพสำหรับการตรวจวัดอัลดีไฮด์สายยาวในน้ำ เช่นเซอรันนาโนนี้พิสูจน์ให้เห็นว่ามีความรวดเร็วและมีความไวสูงในการตรวจวัดอัลดีไฮด์สายยาวโดยเฉพาะอย่างยิ่งออกทานาลและโนนนานาล นอกจากนี้เซ็นเซอร์ระดับนาโนมีความไวสูงในการตรวจวัดโนนนานาล โดยมีขีดจำกัดการตรวจวัดเชิงคุณภาพ (LOD) ที่ 41 ไมโครโมลาร์ และขีดจำกัดการตรวจวัดเชิงปริมาณ (LOQ) ที่ 275 ไมโครโมลาร์ และเวลาในการตรวจวัดที่ 2 นาที ในสารละลายบัฟเฟอร์อะซิเตดที่พีเอช 5 นอกจากนี้เซ็นเซอร์ระดับนาโนยังสามารถใช้ตรวจวัดโนนนานาลได้ด้วยตาเปล่า เช่นเซ็นเซอร์ระดับนาโนที่พัฒนาขึ้นนี้อาจมีศักยภาพสำหรับการตรวจวัดอัลดีไฮด์สายยาวด้วยความจำเพาะเจาะจงและความไวสูงในน้ำ

จุฬาลงกรณ์มหาวิทยาลัย
CHULALONGKORN UNIVERSITY

สาขาวิชา เคมี

ลายมือชื่อนิติกร

ปีการศึกษา 2565

ลายมือชื่อ อ.ที่ปรึกษาหลัก

6470124823 : MAJOR CHEMISTRY

KEYWORD Long-chain aldehydes, Naphthalimide dyes, Ethyl cellulose,
D: Fluorescence nanosensor, encapsulating, EC@Naph

Faiza Lawan Isah : FLUORESCENT HYDRAZINE-NAPHTHALIMIDE ENCAPSULATED BY ETHYL CELLULOSE FOR DETECTION OF LONG-CHAIN ALDEHYDES. Advisor: Assoc. Prof. BOOSAYARAT TOMAPATANAGET, Ph.D.

One of the most common diseases globally which takes numerous lives is lung cancer. The high concentrations of aldehydes found in tobacco smoke and motor vehicle exhaust are among the contributors for lung cancer. There is a lot of interest in developing a nanosensor for identifying long-chain aldehydes. The conventional methods for detecting aldehyde are highly complex, expensive, and time-consuming. To overcome this drawback, alternative detection techniques such as fluorescence techniques are needed for the quick, easy, and affordable identification of aldehydes. Aldehyde molecules and their derivatives are often used as biomarkers to aid in the diagnosis and treatment of lung cancer patients. This property has been exploited to design an effective nanosensor for identification of long-chain aldehydes. In this study, we created a water-soluble fluorescence nanosensor based on dye-encapsulated polymeric nanoparticles consisting of naphthalimide and ethyl cellulose (namely EC@Naph). According to fluorescence results, the EC@Naph demonstrated excellent performance for recognising long-chain aldehydes. Notably, it offered rapid detection and good sensitivity to octanal and nonanal. This sensing platform showed a limit of detection (LOD) of 41 μM and a limit of quantification (LOQ) of 275 μM , towards nonanal sensing in acetate buffer with a pH of 5.0 with a reaction time of 2.0 min. Interestingly, this sensing platform can perform naked-eyed sensing for nonanal. Expectedly, the developed nanosensor possesses a high degree of selectivity and sensitivity for detection of nonanal in aqueous media.

Field of Study:	Chemistry	Student's Signature
Academic Year:	2022
		Advisor's Signature
	

ACKNOWLEDGEMENTS

My greatest appreciation goes to my supervisor, Associate Professor Boosayarat Tomapatanaget, Ph.D., for her guidance, advice, reading, and corrections to see this thesis succeed. May God reward her abundantly, bless her family and make her successful in this world and hereafter.

I want to express my appreciation to Professor Dr. Patchanita Thamyongkit, Professor Dr. Thawatchai Tuntulani, Associate Professor Dr. Fuangfa Unob and Dr. Thanthapatra Bunchuy who were my thesis committee members for their suggestions, recommendations, and advice. May God bless you all.

I also acknowledge the financial support by Chulalongkorn University Graduate Scholarship for ASEAN and Non-ASEAN Countries.

I would like to thank all my lab members and Supramolecular Chemistry Research Unit (SCRU) members for their contribution to the success of this thesis. My special thank goes to P'Gig for her mentorship. I wish her all the best in all her activities.

To my family, there is no word I can express my gratitude to them; I say May Allah reward them abundantly, Ameen.

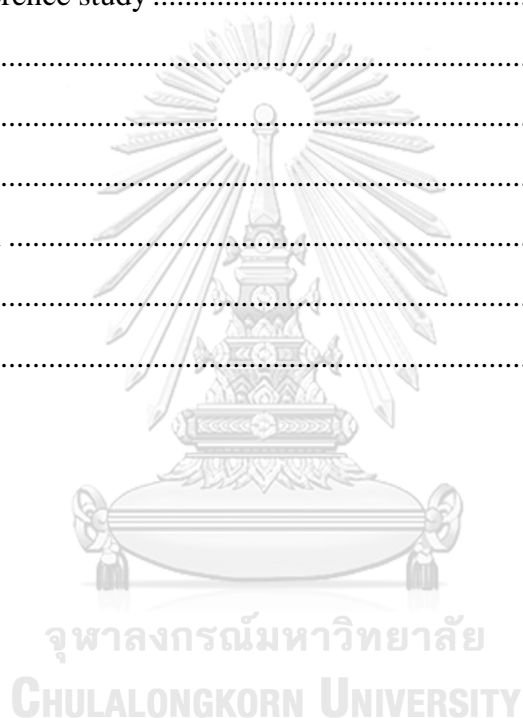
Faiza Lawan Isah

TABLE OF CONTENTS

	Page
ABSTRACT (THAI)	iii
ABSTRACT (ENGLISH).....	iv
ACKNOWLEDGEMENTS.....	v
TABLE OF CONTENTS.....	vi
LIST OF TABLES	ix
LIST OF FIGURES	x
CHAPTER I.....	1
INTRODUCTION AND LITERATURE REVIEWS.....	1
1.1 Introduction	1
1.1.1 Supramolecular chemistry.....	1
1.1.2 Fluorescence.....	2
1.1.3 Aldehyde compounds and their sensing.....	7
1.1.4 Amine functionalised sensors for aldehydes detection	11
1.1.5 Nanoparticles.....	16
1.2 Research objective.....	21
1.3 Benefit of this research.....	22
CHAPTER II.....	23
EXPERIMENTAL.....	23
2.1 General procedure	23
2.1.1 Analytical instruments.....	23
2.1.2 Materials.....	23
2.2 Synthesis of naphthalimide dye (Naph)	24
2.3 Preparation of dye-encapsulated ethyl cellulose (EC@Naph) nanosensors.....	25
2.4 Characterization of EC@Naph nanosensors	26
2.4.1 Element analysis of EC@Naph nanosensors	26

2.4.2 Dynamic light scattering (DLS) of EC@Naph nanosensors	27
2.4.3 Zeta potential measurement of EC@Naph nanosensors	27
2.5 Optical studies of EC@Naph nanosensors	27
2.5.1 Fluorescence studies of the EC@Naph nanosensors.....	27
2.5.2 Stability study of EC@Naph nanosensors	28
2.6 Selectivity studies of Naph dyes towards aldehyde families.....	28
2.7 Optimisation of the EC@Naph nanosensors for long-chain aldehydes detection	29
2.7.1 pH investigations of EC@Naph nanosensors in micellar platforms for	
nonanal detection.....	29
2.8 Selectivity test of EC@Naph nanosensors towards detection of various	
aldehyde compounds	29
2.9 Quantitative analysis of EC@Naph nanosensors for nonanal detection	31
2.10 Quantitative investigation of EC@Naph with nonanal by visual detection	
34	
2.11 Interference studies of EC@Naph nanosensors	34
CHAPTER III	37
RESULT AND DISCUSSION	37
3.1 Design Concept of Naphthalimide encapsulated sensors for Long-Chain	
Aldehydes detection	37
3.2 Synthesis and characterization of Naphthalimide (Naph)	39
3.3 Preparation of fluorescence dye-encapsulated by ethyl cellulose nanosensors.	41
3.4 Characterization of Naph encapsulated by ethyl cellulose (EC@Naph).....	42
3.4.1 Fourier transform infrared spectroscopy (FT-IR)	42
3.4.2 Scanning electron microscopy coupled energy dispersive x-ray	
spectroscopy (SEM-EDX).....	43
3.4.3 Optical property study of EC@Naph nanosensor	45
3.5 The stability study of EC@Naph nanosensors	45
3.6 Dynamic light scattering (DLS) and zeta potential studies	46
3.7 Investigation into the reaction time of EC@Naph with nonanal.....	49
3.8 Sensing properties of EC@Naph towards nonanal	50

3.9 Optimization of the sensing system for long-chain aldehydes detection	52
3.9.1 Study on pH effect of EC@Naph nanosensors for long-chain aldehydes detection	53
3.10 Selectivity of EC@Naph nanosensors.....	54
3.11 The interaction study between EC@Naph with nonanal by fluorescence titration	59
3.12 Quantitative Analysis of EC@Naph for Nonanal Detection Using Naked- Eye Observation	61
3.13 Interference study	61
CHAPTER IV	63
CONCLUSION.....	63
4.1 Conclusion.....	63
4.2 Future work	64
REFERENCES	65
VITA.....	79



LIST OF TABLES

	Page
Table 2.1 Preparation of EC@Naph nanosensors by various ratios of EC and Naph.	26
Table 2.2 The variation in buffer at various pH levels.	29
Table 2.3 The preparation of 0.06 M stock solution of aldehyde family as guests at 10.00 mL.	30
Table 2.4 Fluorescence settings for measuring selectivity for all EC@Naph nanosensor prepared in various ratios.	31
Table 2.5 The preparation of nonanal compound at a 10 mM concentration in 10.00 mL.	32
Table 2.6 The concentration of nonanal in EC@Naph nanosensors system.	33
Table 2.7 Conditions for the fluorescence of EC@Naph nanosensors made with a 1:1 mixture of EC and Naph in an aqueous media for a quantification study of nonanal detection.	34
Table 2.8 The preparation of a 10.00 mL final volume 20 mM stock solution of aldehyde and a crucial representative components in blood and exhaled breath.	35
Table 3.1 Hydrodynamic diameter of particle, polydispersity index (PDI) and zeta potential measurement of EC@Naph nanosensors with and without nonanal (C9) guest molecule ⁹	48

LIST OF FIGURES

	Page
Figure 1.1 Schematic representation of supramolecular interaction.....	1
Figure 1.2 Jablonski diagram describing the fluorescence process ¹⁸	3
Figure 1.3 Probe mechanism for formaldehyde detection.	4
Figure 1.4 Conceptual illustration of the sensor for formaldehyde sensing ²¹	5
Figure 1.5 The probe fluorescence turn-on mechanism towards long-chain aldehydes ²²	6
Figure 1.6 Resorcinol functionalised nanoparticle for FA detection.	6
Figure 1.7 General chemical structure of aldehyde compounds.....	7
Figure 1.8 SERS spectra of the grooming product under enhancing substrate using Au nanoparticles for formaldehyde detection ⁶¹	8
Figure 1.9 Responses of formaldehyde and acetaldehyde from flame ionization detection approach.	10
Figure 1.10 Chromatogram of long-chain aldehydes from urine of lung cancer patient.	11
Figure 1.11 Mechanism of hydrazone bond formation ⁶⁶	12
Figure 1.12 Probe detection mechanism for HCHO sensing.	12
Figure 1.13 Probe mechanism for aldehyde detection.	13
Figure 1.14 The ratiometric probe design for FA imaging.....	14
Figure 1.15 Conceptual representation of the colorimetric sensor array.	15
Figure 1.16 Conceptual design of pillar [5] arene based derivative sensor.	16
Figure 1.17 Various classifications of Nanomaterials ⁷⁸	18
Figure 1.18 illustration of the colorimetric sensor array for aldehydes detection.	19
Figure 1.19 Design and Preparation of self-assembly Chitosan- based nanoparticle for FA detection.....	20
Figure 1.20 Sensing mechanism by zeolite nanoparticle.....	21
Figure 3.1 Structures of Naphthalimide-based hydrazine (Naph) a) and Ethyl cellulose polymer (EC) b)21.	38

Scheme 3.1. Conceptual design of the EC@Naph sensing platform for the detection of long-chain aldehydes22.	39
Figure 3.2 Synthesis of Naphthalimide dye (Naph)23.....	39
Figure 3.3 ¹ H NMR spectrum of compound 124.	40
Figure 3.4 ¹ H NMR spectrum of Naphthalimide dye (Naph)25.....	41
Figure 3.5 Design of EC@Naph nanosensor with respect to long-chain aldehydes detection26.	42
Figure 3.6 ATR-FTIR spectra of ethyl cellulose (EC, blue), EC@Naph nanosensor (Magenta) and that of Naphthalimide dye (Naph, orange)27.....	43
Figure 3.7 SEM-EDX map of EC@Naph nanosensor28.....	44
Figure 3.8 EDX Spectrum of EC@Naph29.....	44
Figure 3.9 Absorbance (Abs) left, and fluorescence emission (Em) intensities right of EC@Naph nanosensors in aqueous media30.....	45
Figure 3.10 A Plot showing the stability of EC@Naph nanoparticle at $\lambda_{em} = 550$ nm over 1 month at 2-5°C ($\lambda_{ex} = 450$ nm, PMT 650 V, slit 10nm)31.	46
Figure 3.11 Dynamic light scattering (DLS) measurement of EC@Naph without and with nonanal (C9)32.	48
Figure 3.12 Zeta potential measurement of EC@Naph with and without nonanal (C9)33.	49
Figure 3.13 Reaction time variation of EC@Naph nanosensors with nonanal (C9) (2mM stock in DMSO) guest molecule34.....	50
Figure 3.14 The reaction mechanism involved in the formation of imine bond ⁶⁶ 35..	51
Figure 3.15 Fluorescence spectra of Naph (5 μ M in acetone) in presence of various aldehydes in 5% DMSO/acetate buffer pH 5.0 (λ_{ex} =455, slit=5 and PMT= 600) a) and under a 365 nm fluorescence lamp, the addition of different aldehyde species (2 mM in DMSO) resulted in distinct changes in the visual fluorescence of the Naph dye. The tested aldehyde species included blank (Naph), formaldehyde (C1), propanal (C3), butanal (C4), pentanal (C5), hexanal (C6), heptanal (C7), octanal (C8), and nonanal (C9). These experiments were conducted in a 20 mM acetate buffer with a pH of 5.0 (b)36.....	52
Figure 3.16 Fluorescence intensity of EC@Naph nanosensors in the absence and presence of nonanal (2 mM in DMSO). The buffer solutions used were pH 3.0 citric buffer, pH 4.0 and 5.0 acetate buffer, and pH 6.0, 7.0, 7.4, and 8.0 phosphate buffer (PBS). The measurements were made using a wavelength for excitation (λ_{ex}) of 450	

nm, PMT 600 V, and a slit of 5 nm a) and Fluorescence spectra of EC@Naph nanosensors in the absence and presence of nonanal b)37.	54
Figure 3.17 (a) Fluorescence spectra and (b) enhancement of relative fluorescence intensity ($I-I_0$) of EC@Naph prepared in aqueous solution with a 0.5:1.0 ratio of EC to Naph. The measurements were conducted in acetate buffer (20 mM, pH 5.0) in the presence of various aldehyde compounds (2 mM in DMSO). Upon 450nm excitation, 550 V PMT and 5 nm a slit width. The error bar represents the results obtained from at least three measurement values38.	56
Figure 3.18 (a) Fluorescence spectra and (b) enhancement of relative fluorescence intensity ($I-I_0$) of EC@Naph prepared in aqueous solution with a 1.0:1.0 ratio of EC to Naph. The measurements were conducted in acetate buffer (20 mM, pH 5.0) in the presence of various aldehyde compounds (2 mM in DMSO). Upon 450nm excitation, 550 V PMT and 5 nm a slit width. The error bar represents the results obtained from at least three measurement values39.	56
Figure 3.19 (a) Fluorescence spectra and (b) enhancement of relative fluorescence intensity ($I-I_0$) of EC@Naph prepared in aqueous solution with a 1.5:1.0 ratio of EC to Naph. The measurements were conducted in acetate buffer (20 mM, pH 5.0) in the presence of various aldehyde compounds (2 mM in DMSO). Upon 450nm excitation, 550 V PMT and 5 nm a slit width. The error bar represents the results obtained from at least three measurement values40.	57
Figure 3.20 (a) Fluorescence spectra and (b) enhancement of relative fluorescence intensity ($I-I_0$) of EC@Naph prepared in aqueous solution with a 2.0:1.0 ratio of EC to Naph. The measurements were conducted in acetate buffer (20 mM, pH 5.0) in the presence of various aldehyde compounds (2 mM in DMSO). Upon 450nm excitation, 550 V PMT and 5 nm a slit width. The error bar represents the results obtained from at least three measurement values41.	57
Figure 3.21 Fluorescence images of EC@Naph nanosensors with the addition of different aldehyde species (2 mM in DMSO) including the blank (EC@Naph), (C1) formaldehyde, (C3) propanal, (C4) butanal, (C5) pentanal, (C6) hexanal, (C7) heptanal, (C8) octanal, and (C9) nonanal. The measurements were conducted in 20 mM acetate buffer at pH 5.0 under a 365 nm UV irradiation42.	59
Figure 3.22 (a) Fluorescence spectra and (b) plot illustrating the enhancement of relative fluorescence intensity ($I-I_0$) of EC@Naph in an aqueous solution with a 1.0:1.0 ratio of EC to Naph. The measurements were performed upon the addition of different nonanal concentrations ranging from 0.0 to 500 μ M in acetate buffer (20 mM, pH 5.0)43.	60

Figure 3.23 Fluorescence images of EC@Naph nanosensors (3.5% v/v) obtained by adding different concentrations of nonanal (in DMSO): blank (EC@Naph), (I) 1 μM , (II) 5 μM , (III) 10 μM , (IV) 50 μM , (V) 100 μM , (VI) 1.0 mM, and (VII) 1.5 mM. The measurements were conducted in 20 mM acetate buffer at pH 5.0 under a 365 nm UV lamp⁴⁴.....61

Figure 3.24 (a) Fluorescence intensity and (b) plot illustrating the relative fluorescence responses of EC@Naph upon the addition of nonanal (500 μM in DMSO) alongside short-chain aldehyde species and major plasma and lung fluid compounds (500 μM in DMSO) in acetate buffer (20 mM, pH 5.0). The findings were made using λ_{em} of 450 nm, a PMT of 650 V, and a slit of 10 nm⁴⁵.....62



CHAPTER I

INTRODUCTION AND LITERITURE REVIEWS

1.1 Introduction

1.1.1 Supramolecular chemistry

A growing area of science called supramolecular chemistry concentrates on a small group of molecules which are connected together through relatively feeble chemical interactions, including electrostatic charges, hydrogen bonds, and Van der Waals forces. Hydrophobic forces, and π - π interactions are a few more interactions that can be presented in a supramolecular system. The enzyme-substrate mechanism Emil Fischer developed in 1894 using a key and lock mechanism. The discovery of supramolecular chemistry began with the finding of two (2) key mechanisms, molecular recognition and supramolecular function. Complex chemical systems are built using noncovalent interactions in supramolecular chemistry. Molecular folding, host-guest interactions, and molecule self-assembly and recognition are some of the most notable characteristics of supramolecular chemistry. As Jean-Marie Lehn pointed out, the creation of a supramolecular system is characterized by three distinct characteristics that are vitally important even though they do not have to be present simultaneously. In light of the fact that all life on Earth has evolved through self-organization or self-assembly, it is essential for self-assembled components. The following categories were used to group the topics in supramolecular chemistry such as molecular interactions as in **Figure 1.1**, complexation, self-assembly, and a molecular recognition. This covers a variety of subjects, comprising biologically produced units, template-directed synthesis, and synthetic recognition motifs¹⁻¹³.

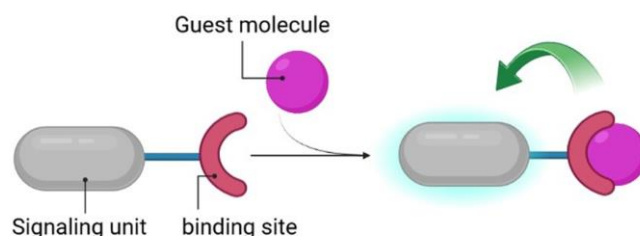


Figure 1.1 Schematic representation of supramolecular interaction.

Furthermore, supramolecular chemistry encompasses the Inorganic and organic chemistry in which both of them fall within the broad realm of chemistry; The creation of sensory molecules with specialised recognition sites, investigations into the ways that host-guest molecules self-assemble, and use of common components. The supramolecular approach has currently been widely adopted in a range of sectors, including catalysis, medicinal therapies, and intelligent material technologies.

1.1.2 Fluorescence

When an electronic system moves from an excited state to the ground state, it emits light, which is known as luminescence. Crystallization, mechanical action on substances, chemical reactions, and living creatures are all potential sources of luminescence. Fluorescence and phosphorescence are conceptually two different forms of luminescence that can be divided based on their excited states and ground states¹⁴⁻¹⁶. The absorption, fluorescence, and phosphorescence processes are depicted in the Jablonski diagram (**Figure 1.2**). In the fluorescence an electron at the ground state S_0 is excited to a higher singlet state (S_1, S_2, \dots, S_n) upon photon absorption ($h\nu$). After that, a vibrational relaxation (or internal conversion, IC) occurs from higher vibrational state to lower vibration state and go back to the ground state. The energy decayed from S_1 to S_0 during the process is referred to as fluorescence as in **Figure 1.2**. Moreover, in phosphorescence the excited state electron went to excited state without changing the spin, intersystem crossing to a triplet state (radiation-less) which causes the spin of electron to invert. Hence, orientation of the electrons in the ground state and the triplet state is the same. Radiative decay to S_0 then follows vibrational relaxation. According to quantum physics, such a decay process involves a forbidden transition, making phosphorescence less likely to occur than fluorescence. For phosphorescence, the decay constants are greater¹⁷.

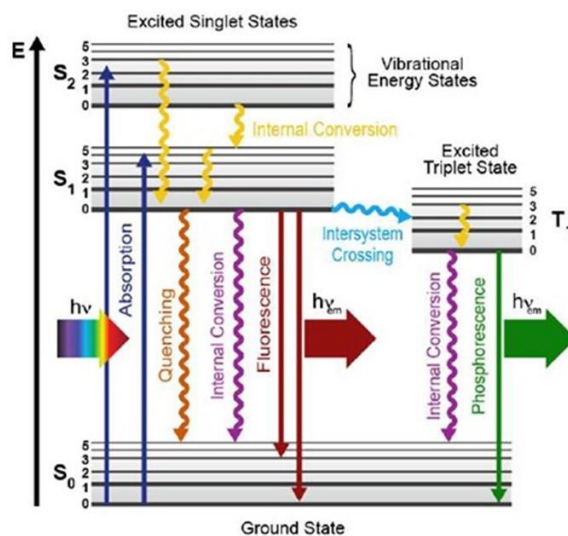


Figure 1.2 Jablonski diagram describing the fluorescence process ¹⁸.

The fluorescent approach offers numerous benefits over conventional sensors, including non-destructiveness, excellent biocompatibility, high sensitivity, and simplicity of usage ¹⁹. Numerous aldehyde detection probes have been created over the past few decades.

A novel fluorescent probe that depends on the covalent post-synthetic modification (PSM) of University Institute of Oslo-66-NH₂ (UiO-66-NH₂) by naphthalimide (NI) was created and developed by Li et al in 2023 ²⁰. Due to the covalent PSM and metal-organic frameworks (MOFs) combination, the probe has a considerable amount of exposed hydrazine group, which results in remarkable formaldehyde (FA) sensing capability with a low detection limit. When the covalent bonds are present, strong interactions can lock the fluorophore and stop it from exhibiting aggregation-induced emission (AIE). The probe can also be utilized in investigations with real samples. Additionally, Forster resonance energy transfer (FRET) is suggested as the main mechanism of fluorescence quenching by experimental findings. As seen in **Figure 1.3** The quenching mechanism for the reaction of the probe with FA is as described on the left, and the unique properties of UiO-66-HN, such as its high sensitivity and AIE traits, are described on the right.

However, this sensor is unable to distinguish between long-chain, aromatic, and low molecular mass aldehydes.

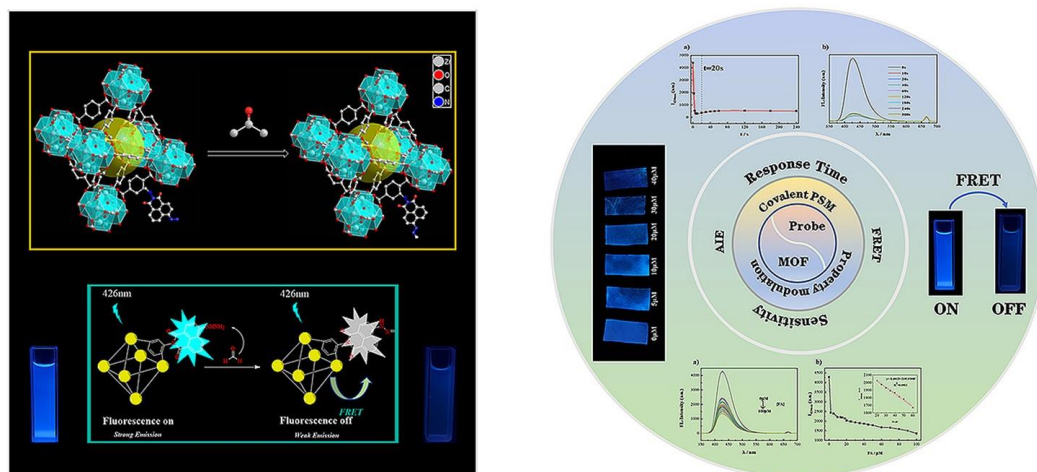


Figure 1.3 Probe mechanism for formaldehyde detection.

For the visual detection and on-site monitoring of formaldehyde (FA) in foods and living cells, a novel pyrene-based ratiometric fluorescence sensor (PN) was created by Hu in 2023²¹. As shown in **Figure 1.4**, the sensor encountered a particular 2-aza-Cope rearrangement towards FA and produced a considerable monomer to excimer conversion in a ratiometric way. High sensitivity, quick response, and successful FA assessment in actual food samples were all characteristics of this sensor PN. Notably, FA in liquid and gaseous states were detected visually using portable devices which were built using paper-based and alginate gel-based materials. The recovery ranges from 100.01% to 100.06% and 99.93% to 99.98%, respectively. Different concentrations of FA in liquid and vapour could be precisely determined using the devices. These findings suggested that the sensing approach may produce a precise and concurrent quantitative study of FA. Unfortunately, this sensor cannot discriminate long-chain aldehydes.

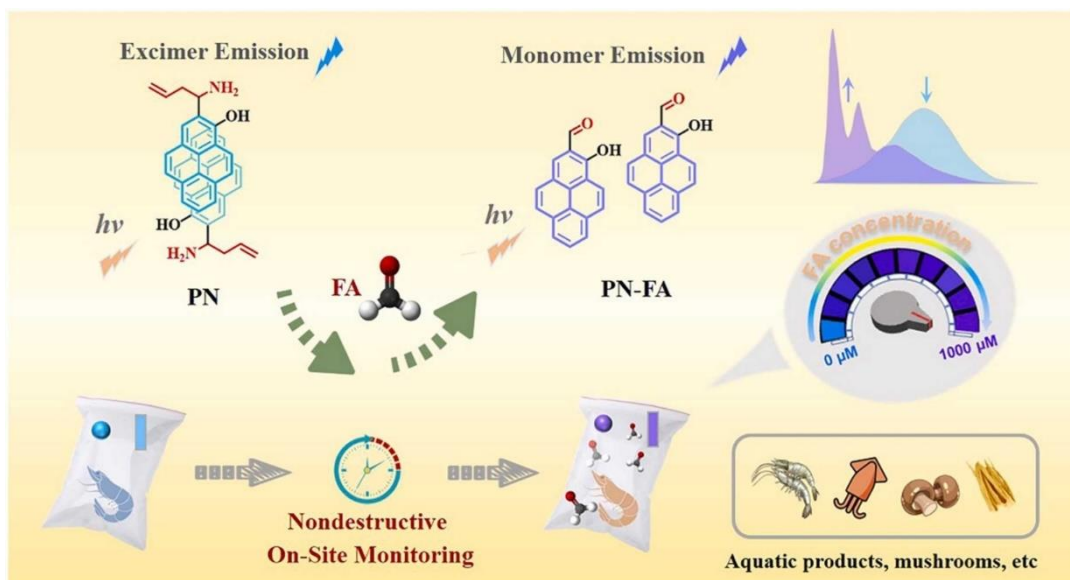


Figure 1.4 Conceptual illustration of the sensor for formaldehyde sensing ²¹.

In 2020, a turn-on fluorescent probe was created using BODIPY molecule by Wang and co-workers ²². The photo-induced electron transfer (PET) process of the BODIPY is inhibited by the reaction of BODIPY with fatty aldehyde which resulted in turn on process as shown in **Figure 1.5**. This concept is utilized to detect long-chain aldehydes present in six edible vegetable oils. The probe responded quickly and sensitively to saturated fatty aldehydes in acetonitrile, producing a dramatic "turn-on" fluorescence. Pre-column derivatization fluorescence by high-performance liquid chromatography was used to build a very sensitive detection technique for long-chain fatty aldehydes. The established chromatographic technique offered adequate precision, a low detection limit, good linearity, and satisfactory precision. The probe may be utilized in regular analysis to determine the kind of vegetable oil for excellent reliability. However, this method is complicated.

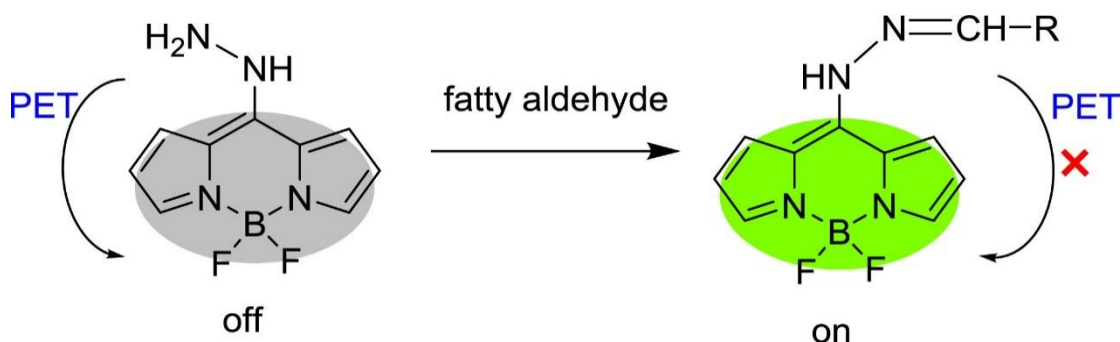


Figure 1.5 The probe fluorescence turn-on mechanism towards long-chain aldehydes²².

In 2019, Carlos and co-workers²³ synthesized an easy formaldehyde sensor made of an aqueous dispersion of gold nanoparticles functionalized with resorcinol. The probe was employed to directly detect formaldehyde in aqueous media and gas phases. The terminal resorcinol and formaldehyde moieties condense in the reaction which provides the detection process. As a result, the scattered nanoparticles start to aggregate resulting in colour change from red to blue (**Figure 1.6**). The probe can be used to detect formaldehyde emissions coming from wood composite boards with low detection limit. However, the probe cannot discriminate long-chain aldehydes.

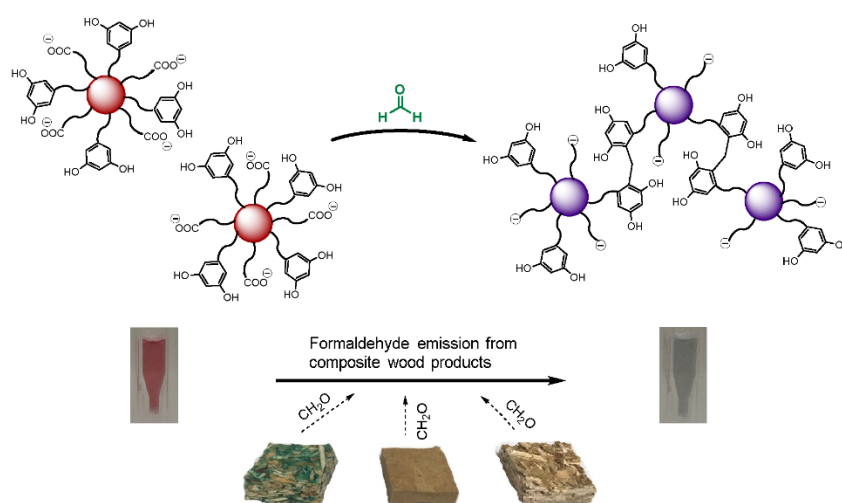


Figure 1.6 Resorcinol functionalised nanoparticle for FA detection.

1.1.3 Aldehyde compounds and their sensing

Aldehydes are a subclass of organic materials whereby a carbon atom make double bonds with oxygen and single bond with hydrogen with respect to additional atoms or groups of atoms (marked R in chemical structures as in **Figure 1.7**). All aldehydes have what is known as a carbon-oxygen double bond is formed referred to as carbonyl group. Many aldehydes have odours that are pleasing, and in theory, they are form through dehydrogenating (removal of hydrogen) from alcohols, which is the origin of the word "aldehyde". In most basic aldehyde family (formaldehyde), the carbonyl group is joined to a pair of hydrogen atoms. In condensed structural formulae, the carbonyl group of an aldehyde is commonly represented as -CHO as in **Figure 1.7**. Aldehyde carbon atoms may be connected to aromatic, alkyl groups (saturated or unsaturated), and heterocyclic rings. Otherwise, they may be free-floating carbon atoms ²⁴. Aldehydes are present everywhere in the natural world. Examples of aldehydes that are found in smoke from cigarettes include formaldehyde, acetaldehyde, and acrolein ²⁵. These compounds are produced during burning. Moreover, a variety of aliphatic and aldehydes can be found in various foods, particularly in fruits and vegetables such as formaldehyde, benzaldehyde, nonanal, malondialdehyde, acrolein, 4-Hydroxynonenal, glyoxal, crotonaldehyde, methylglyoxal, citral and so on. Aldehydes are categorized as human carcinogens, which can cause a variety of illnesses, including cancer and Alzheimer's disease. Long-chain aldehydes have been recognized as long-term cancer indicators due to their lengthy alkyl chains ²⁶⁻³¹.

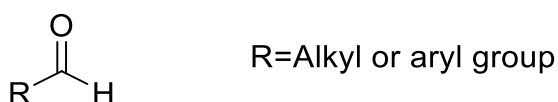


Figure 1.7 General chemical structure of aldehyde compounds.

Numerous analytical studies have been conducted to identify aldehyde molecules and their derivatives. Gas chromatography (GC) ³²⁻⁴⁴, high-performance liquid chromatography (HPLC) ⁴⁵⁻⁵¹, mass spectrometry (MS) ^{52, 53} Raman

spectroscopy⁵⁴, and electrochemical techniques have traditionally been used to study these substances⁵⁵⁻⁶⁰. However, these techniques show excellent sensitivity, selectivity, and determination that is exact and accurate.

Toxic formaldehyde is illegally added as a preservative to grooming items to increase shelf life. In order to identify formaldehyde in grooming products, Nie et al. 2023⁶¹ proposed a Surface-Enhanced Raman Spectroscopy (SERS) method with substrates made of modified trisodium citrate for reduction-produced gold (Au) nanoparticles for the detection of formaldehyde in cosmetics. Formaldehyde has been transformed into an azine molecule which have an excellent surface-enhanced raman spectroscopy activity using a derivatization reagent. The difficulty in the detection of formaldehyde poses a challenge due to its limited Raman scattering cross-section, might be overcome by this. The finding shows that the grooming products contain formaldehyde by employing this method. From 0.4 to 80 mg/kg, more formaldehyde was added to the samples which enhance the intensity of the SERS signals as in **Figure 1.8**. The method shows a good correlation coefficient and an there exists a strong linear correlation for the formaldehyde sensing in toothpaste and shampoo with low detection limits. Due to SERS methodology drawbacks such time-consuming material preparation, high cost, and environmental harm, this technology was unable to reach the optimal position for biosensing fields.

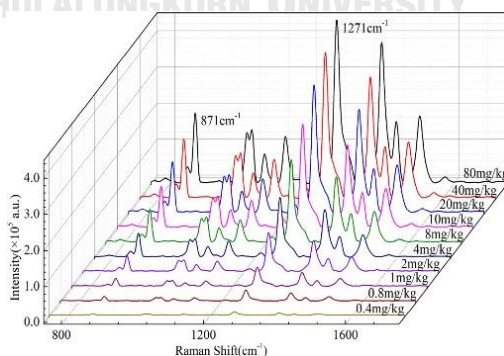


Figure 1.8 SERS spectra of the grooming product under enhancing substrate using Au nanoparticles for formaldehyde detection⁶¹.

Regarding free requirement of sample pre-treatment or concentration, Luong et al. in 2018⁶² effectively create a gas chromatographic (GC) technique whereby formaldehyde and acetaldehyde were successfully detected and quantified in gaseous environments without requiring for any additional equipment, conversion of aldehydes to alkanes using catalytic hydrogenolysis is carried out in the flame ionisation detector's steel jet assembly which was 3D-printed. This method quantified formaldehyde and acetaldehyde in parts-per-million (ppm) levels. It took less than 10 minutes to complete the analysis. Here, the performance of a standard flame ionization detection (FID) jet and a 3D-printed FID jet with catalyst was compared. Similar gas chromatographic and detector conditions applied to both jet operations. As a baseline, formaldehyde and acetaldehyde in nitrogen standards were employed to measure their levels. An increase for formaldehyde count of more than 35 times was observed in the area. The result illustrated the benefit of using the 3D-printed jet for formaldehyde detection. As expected, the influence of catalytic hydrogenolysis in FID response lessened as the aldehyde's carbon chain length increased, leading to an increase in the production of formaldehyde (CHO+) ions. Nevertheless, acetaldehyde showed an increase in response time of more than 1.6 times. There was not a noticeable difference in the methanol reaction. This demonstrates the catalyst's high level of selectivity, which was used to increase the analytes' overall sensitivity by FID as seen in **Figure 1.9**. In contrast, this approach is complex, expensive, and requires a significant amount of time.

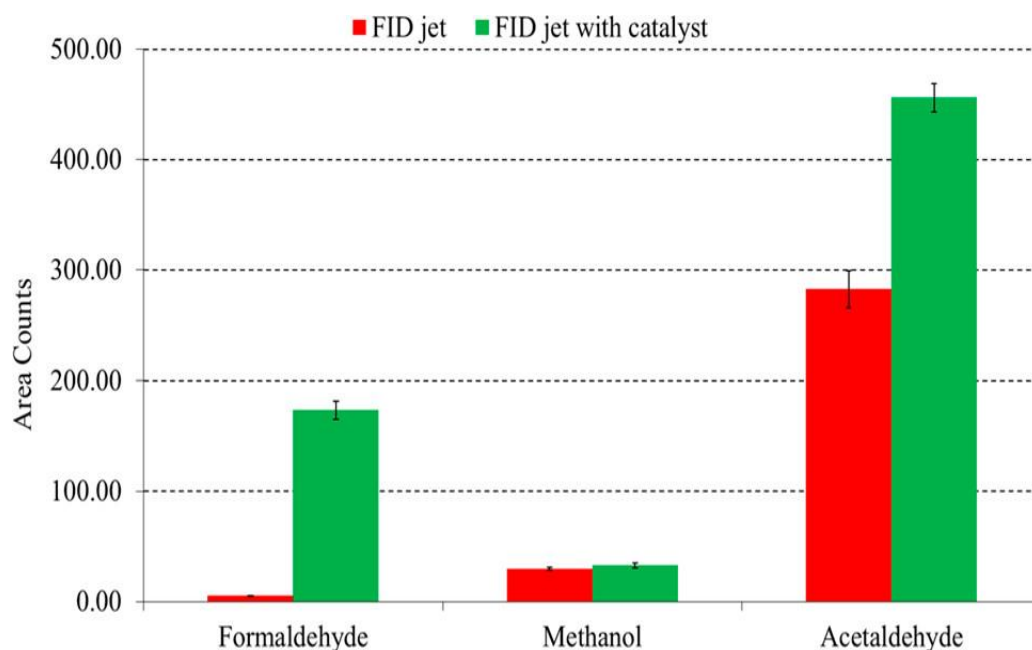


Figure 1.9 Responses of formaldehyde and acetaldehyde from flame ionization detection approach.

To measure hexanal and heptanal levels in urine, a liquid chromatography-mass spectrometry (LC-MS) approach was employed was created by Chen et al in 2017⁶³. The procedure involved combination of liquid chromatography (LC) elute and hydroxylamine hydrochloride (HAHC) solution to achieve post-column derivatization (PCD). Subsequently, long-chain aldehydes (hexanal and heptanal) levels in urine samples were determined using this method that had been designed. In order to test the method's accuracy in measuring endogenous aldehydes, it was then used to analyse 10 urine samples from lung cancer patients. Six samples yielded successful hexanal and heptanal detections. These outcomes demonstrated the viability of fully automated analysis of urine sample aldehydes (**Figure 1.10**). On the other hand, the drawback of this approach is complex, expensive, and time-consuming.

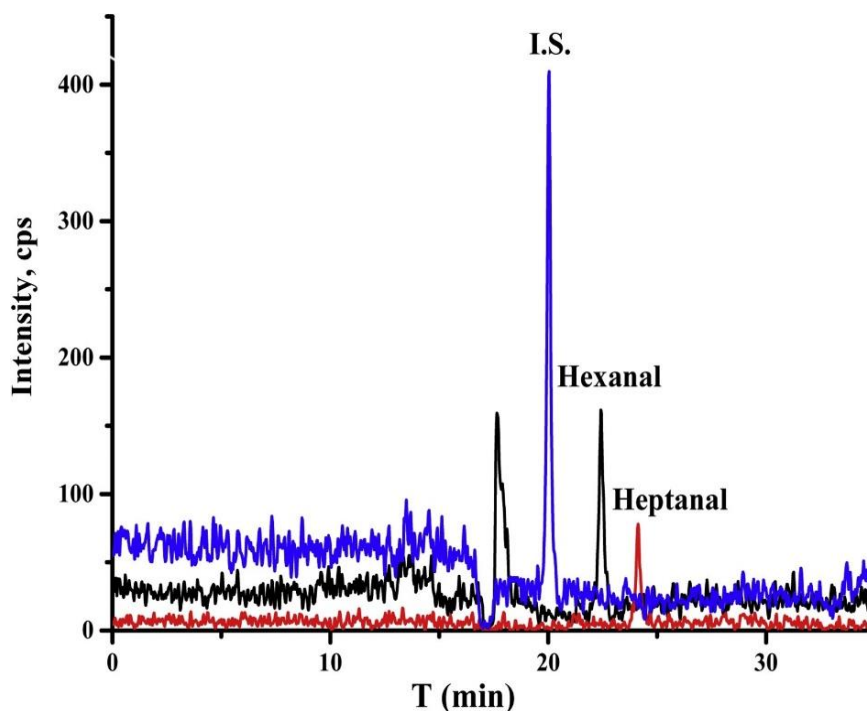


Figure 1.10 Chromatogram of long-chain aldehydes from urine of lung cancer patient.

In summary, these analytical detection techniques have several shortcomings, such as being extremely difficult, costly, and tedious. The fluorescence approach, in contrast, is a remarkably effective analytical technique that has drawn a lot of study interest because of its comparative advantages including excellent selectivity, sensitivity, intrinsic precision, real-time monitoring, and quick response¹⁹. Consequently, There is a substantial and noteworthy interest in the detection of aldehydes utilising fluorescence technique.

1.1.4 Amine functionalised sensors for aldehydes detection

Chemical mechanisms frequently employ the aldehyde's carbonyl group and an external amino group shown in **Figure 1.11** to form the imine bond for responsive aldehydes fluorescence probes with respect to host-guest interaction^{64, 65}.

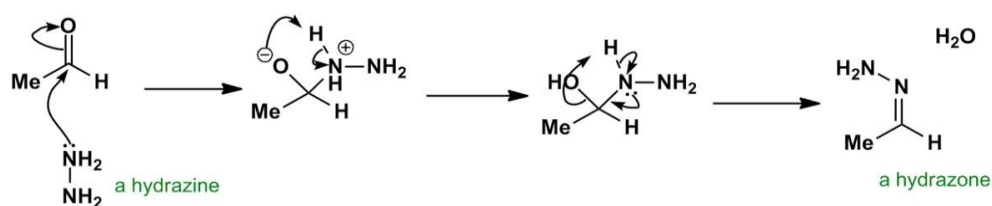


Figure 1.11 Mechanism of hydrazone bond formation ⁶⁶.

Li et al. in 2018 ⁶⁷, presented chitosan (HN-Chitosan) polymer functionalized-hydrazino-naphthalimide as a probe for fluorescence in formaldehyde (HCHO) detection. The probe is a reliable hydrophilic polymeric probe that enables rapid formaldehyde detection present in pure water sample measured in parts-per-million (ppm). Formaldehyde (HCHO) and the reactive site of the hydrazino group interact chemically to provide the "turn-on" fluorescence response of naphthalimide fluorophores of the probe as shown in **Figure 1.12**. HN-Chitosan, the chitosan contained small-molecule-based analogues with a hydrazine group as aldehyde reactive site together with high density of hydroxyl groups as in **Figure 1.12**. This probe features significantly speeds up the reaction between hydrazine group of the probe and HCHO. As a result, a quick fluorescence response with great sensitivity are achieved. Additionally, HN-Chitosan has a sizable linear detection range and decent photostability. Unfortunately, this method cannot detect long-chain aldehydes.

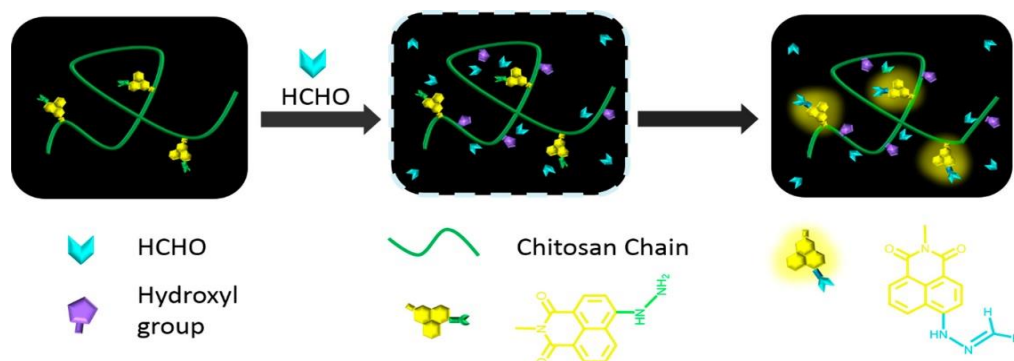


Figure 1.12 Probe detection mechanism for HCHO sensing.

In 2022⁶⁸, a lipophilic naphthalimide fluorescence probe was created by researchers to profile aldehydes during oxidation of lipids as in **Figure 1.13**. The extraction and precipitation method were developed to purify the fluorescent probe. Analysis of the probe's fluorescence characteristics and the Malondialdehyde (MDA) and hexanal, common aldehydes that were condensed to produce these compounds that inhibiting photo-induced electron transfer (PET) after condensation significantly increased the fluorescence intensity. By emitting different fluorescence colours (green for hexanal; blue for MDA), the probe could distinguish between the two compounds. Numerous aldehyde products from oxidation were easily identified by the fluorescent probe when typical unsaturated lipids were aerobically oxidised using high-performance liquid chromatography- mass spectroscopy (HPLC-MS), illustrating the versatility in addition to enormous potential of using this probe to profile aldehydes during the oxidative process of lipids. However, this research is limited by the drawback of complicated material preparation.

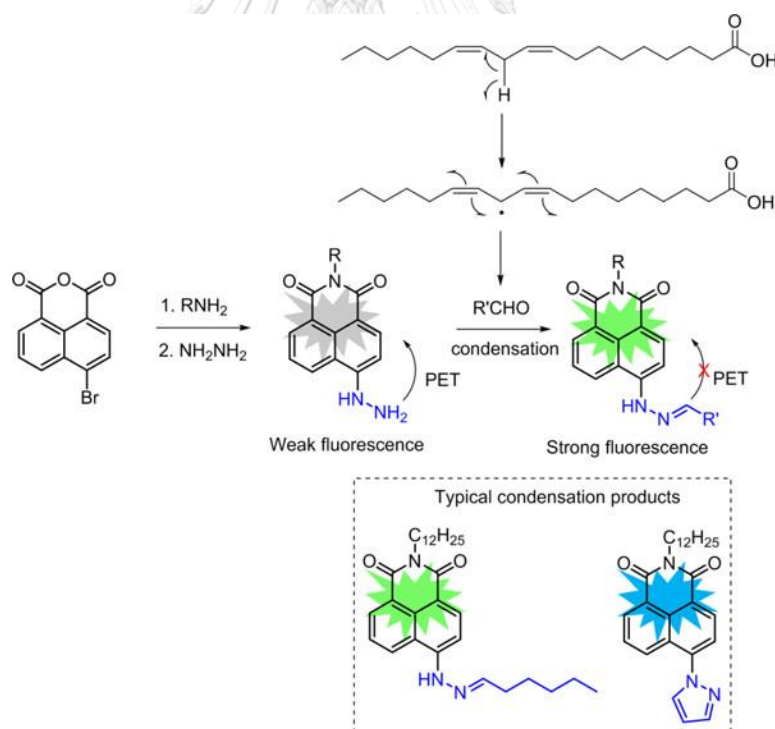


Figure 1.13 Probe mechanism for aldehyde detection.

To enhance aldehyde compound detection abilities, Chen and co-workers in 2019²⁷ have successfully designed a biocompatible ratiometric fluorescence

nanoprobe using carbon dots (CDs) modified with naphthalimide derivatives (ND) to selectively detect formaldehyde (FA) using phosphate (PBS) buffer and live cells (**Figure 1.14**). The nanoprobe is effective for detecting endogenous FA in real systems and functions under normal pH levels. The nanoprobe has an excellent cell penetration, little cytotoxicity, a high ratio of signals to noise, and most importantly, an extremely low limit of detection. The downside of the nanoprobe is that it cannot identify long chain aldehyde.

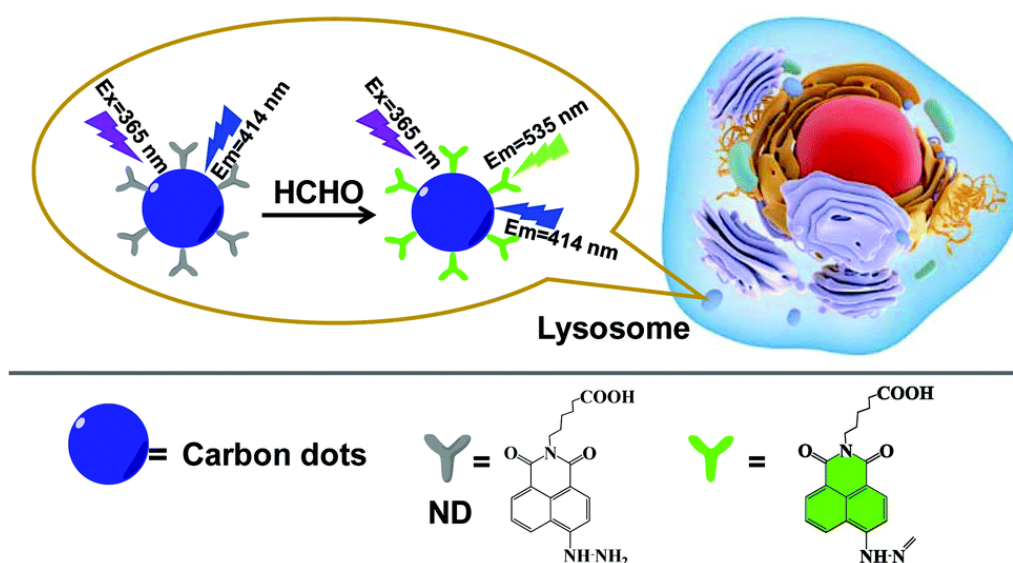


Figure 1.14 The ratiometric probe design for FA imaging.

In order to distinguish between 16 potential hazardous organic lung cancer biomarkers and 9 different types of aldehydes in low concentration, A novel array of colorimetric sensors was created by Li and coworkers (2014)⁶⁹ with regard to an approach that is cross-reactive To serve as specific sensing components, Sixteen from twenty-seven colours of dye were chosen to be combined with 2,4-dinitrophenylhydrazine (DNPH) in an optimised condition, and polyethylene glycol was selected out of four different polyethylene glycols to serve as a stabiliser. The resulting sensor array exhibits better responsiveness to aldehydes and very strong selectivity in low concentrations between 40 ppb and 10 ppm. Both hierarchical cluster analysis (HCA) and discriminant analysis (DA) are utilised to evaluate this data, showing the sensor's exceptional capacity to distinguish between structurally

similar lung cancer-related aldehydes. Additionally, samples of air that had been tainted with formaldehyde were examined using this constructed sensor array, showing a strong possibility of application to the evaluation of these hazardous chemical component. The linear range was precise compared to the theoretical quantification value. The sensor array can be improved in order to monitor formaldehyde in both home and industrial substances settings as well as for the early identification of lung cancer. As illustrated in **Figure 1.15**, H_2SO_4 functions as a catalyst in the reaction between aldehyde and DNPH producing H_2O as a by-product. Changing pH in the H_2O due to a protonation in the sensor dot. The colour shift produced by the dyes will differ from one another because different types and quantities of aldehyde molecules have varied affinities to DNPH and form distinct volumes of H_2O . The optimized dyes are affected to pH variation leading to a colour variation in response. The sensor array's measurement of colour change allows for the differentiation of various aldehydes and other potentially interfering equivalent. Even yet, this sensor's inability to detect significantly long-chains exceeding seven carbon atoms and heavy-weight aldehydes prevented it from distinguishing between a group of aldehydes and other VOCs.

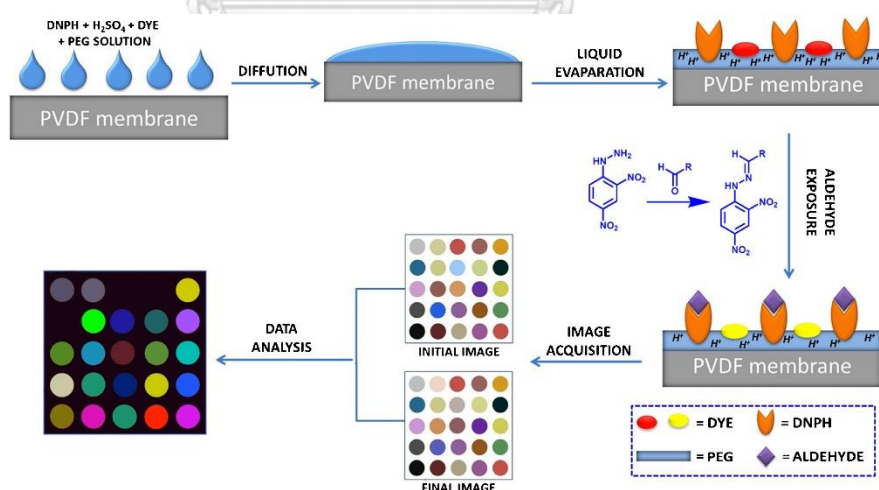


Figure 1.15 Conceptual representation of the colorimetric sensor array.

Lin and coworkers published a novel method in 2018⁷⁰ for the ultrasensitive aggregation-induced emission (AIE) "turn-on" process for formaldehyde (FA)

detection both in gaseous and liquid state utilising a catalyst that replaced macrocycle pillararene based derivative (DP5J-Bi) as a fluorescence sensor as in **Figure 1.16**. DP5J-Bi sense FA with high selectivity and sensitivity by AIE behaviour within 7.5s reaction time. For FA, the experimental limit of detection (LOD) is 3.27×10^{-9} M. Hence this unique method is used to sense FA present in liquid and gas. Moreover, this method allows effective detection of additional volatile organic chemicals. Unfortunately, this method cannot detect higher molecular weight aldehydes based on aromatic aldehydes.

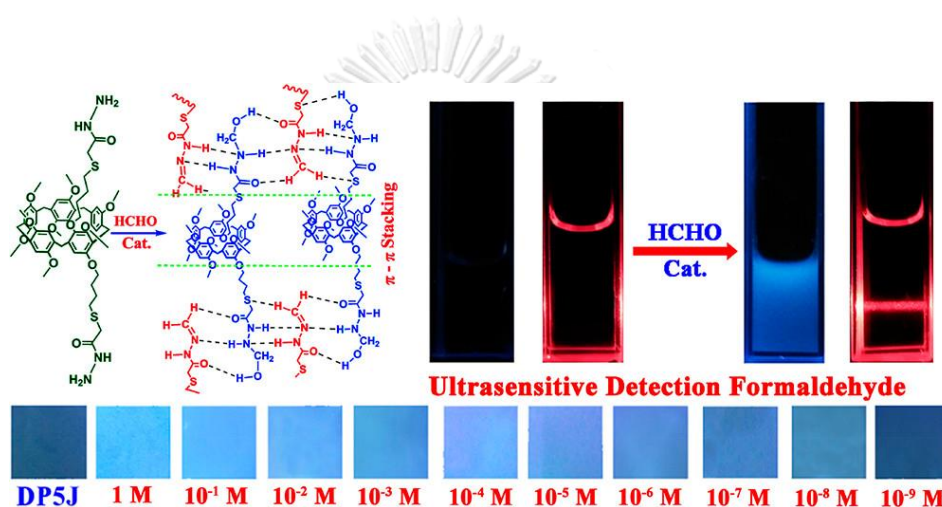


Figure 1.16 Conceptual design of pillar [5] arene based derivative sensor.

1.1.5 Nanoparticles

Nanomaterials (NMs) can be used in the aldehydes sensing investigation in addition to using host and guest binding interaction to detect aldehydes. The Greek word for “dwarf,” nano, is used to describe it. Given that the substance has very small size (1nm) which make it invisible to the human eye⁷¹. To put it in simply, nanostructures are ultrafine particles having dimensions between a few to 100 nm. Nanoparticles have generated a lot of attention in the field of analytical chemistry due to their significant optical characteristics, surface area relative to volume ratio, chemical durability, excellent ability to adsorb because of their small size, stability at extreme temperatures⁷². Optically active chromogenic or fluorogenic nanoparticles are widely used in the fields that include sensing and bioimaging. Examples include semiconductors quantum dot particles, nanomaterials, nanoparticles made of metal

oxides, colloidal Gold and silver, silicon, dye-doped silica, up transformation, and various other substances.

NMs can be categorized into several groups with respect to their morphology, chemical constituents and moreover their dimensions. The NMs size ranges from 1-100nm. In addition, NMs can be categorized based on the material dimension as in **Figure 1.17**, Nanostructures can exist in various dimensions, including zero dimensions (0D), one dimension (1D), two dimensions (2D), or three dimensions (3D). Specifically, zero dimensional (0D) NMs are class of nanomaterials that have all dimensions less than 100nm (within the nanoscale), example include quantum dots (QDs) and nanoparticle. Furthermore, One-dimension (1D) NMs are a class of nanomaterials that have one dimensions that exceeds the 100nm and two dimensions are within the size of nanoscale. Example of these class of NMs includes nanorods, nanotubes and others. Two-dimensional (2D) NMs are class of nanomaterials having one dimension within the nano range and the other dimensions exceeds the nano range, example include nanocoating, nanofilms and so on. Finally, the three-dimension (3D) NMs are the class of nanomaterials with all their dimensions more than 100nm (exceed the nanoscale), examples of these materials include nanowires, pillars and other ⁷³⁻⁷⁷.

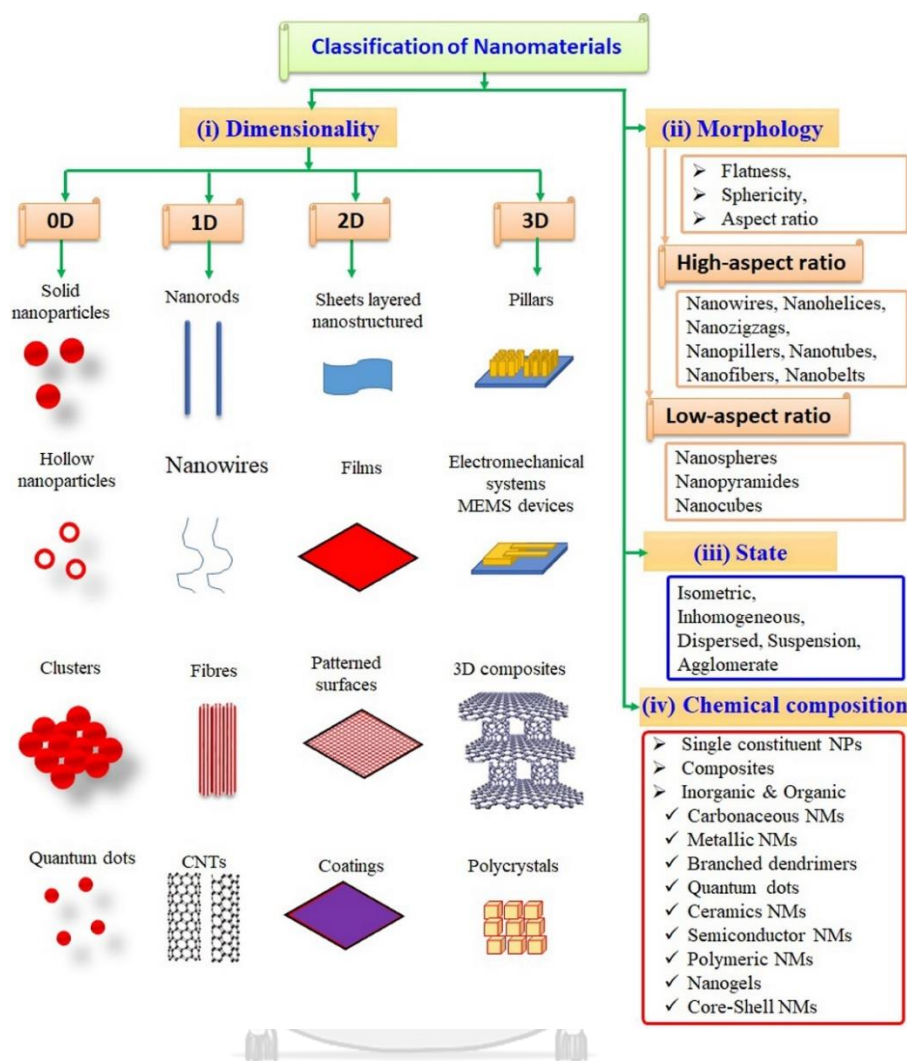


Figure 1.17 Various classifications of Nanomaterials ⁷⁸.

Aldehyde investigation and detection using a colorimetric sensor array was published by Li et al. in 2022 ⁷⁹. There were three different types of gold nanoparticles (Au NPs) that are negatively charged with three different sizes as 13, 22 and 40 nm. The negatively charge surface of Au NPs attracted silver cation (Ag^+) from tollen's reagent in an aldehyde environment. Ag^+ was transformed to silver neutral (Ag^0), resulting in the Au@Ag core-shell nanostructure and a noticeable colour variation as in **Figure 1.18**. The use of transmission electron microscopy allowed for the precise observation of morphological and dimensions changes. Au NPs red, green, and blue colour models' value variations were recorded as an optical signal for later data processing. The system's exceptional discriminating performance for aldehyde identification with a low detection limit was demonstrated by the pattern

recognition results. The array also has quantitative formaldehyde detection capability, selectivity, and reproducibility, which means it has a lot of potential for practical detection. However, this method cannot discriminate long-chain aldehydes, and moreover this method is complex.

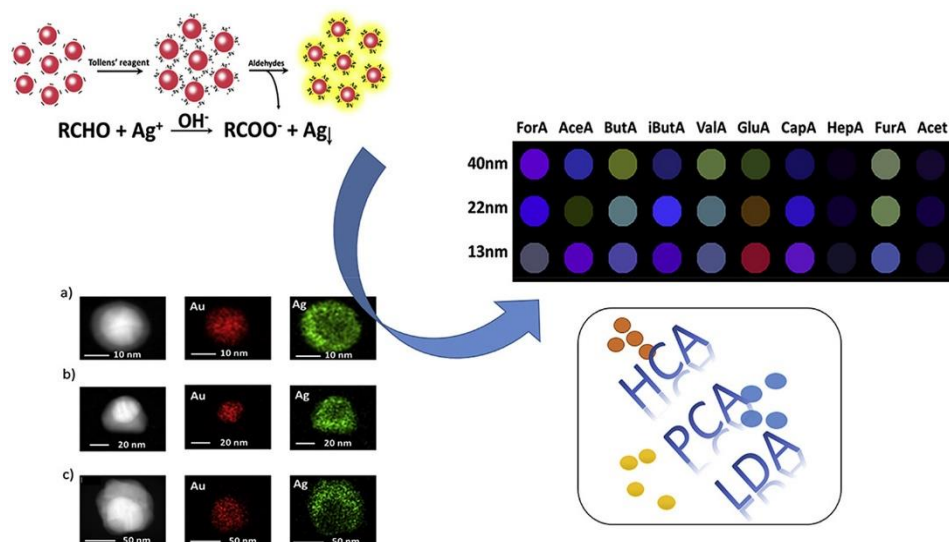


Figure 1.18 illustration of the colorimetric sensor array for aldehydes detection.

Regarding to supramolecular self-assembled ratiometric fluorescent probe, an amphiphilic chitosan (CS) based polymer fluorescent probe was created by Yang and co-workers in 2022⁸⁰. The probe was made by covalent bonding the fluorophore 4-methoxy-1,8-naphthalimide (MONA) with the hydrophilic natural CS. In addition, the 4-hydrazine-1,8-naphthalene (HANA) imide was used as a reactive site to create the hydrophobically small formaldehyde (FA) molecule fluorescent sensor N-butyl-4-hydrazino-1,8-naphthalimide (NBHN). The improved CS-based probe (CS-OCH₃) transformed to amphiphilic CS-based nanoparticle (CS-OCH₃NPs) by self-assembly which has both polar and non-polar behaviour as shown in **Figure 1.19**. The polymer probe CS-OCH₃NPs with hydrophobic (core) and hydrophilic chains (shell) are created. Then, a certain amount of NBHN fluorescent probe employ for FA detection was add of and readily entered the hydrophobic core of CS-OCH₃NPs, finally resulting in CS-OCH₃@NBHN with numerous reaction groups that might speed up the reaction with FA. As predicted, With the ability to recognise FA in aqueous media, the probe demonstrated extremely promising application. The probe, however,

is unable to distinguish between aromatic aldehydes, short-chain aldehydes, and aliphatic long-chain aldehydes.

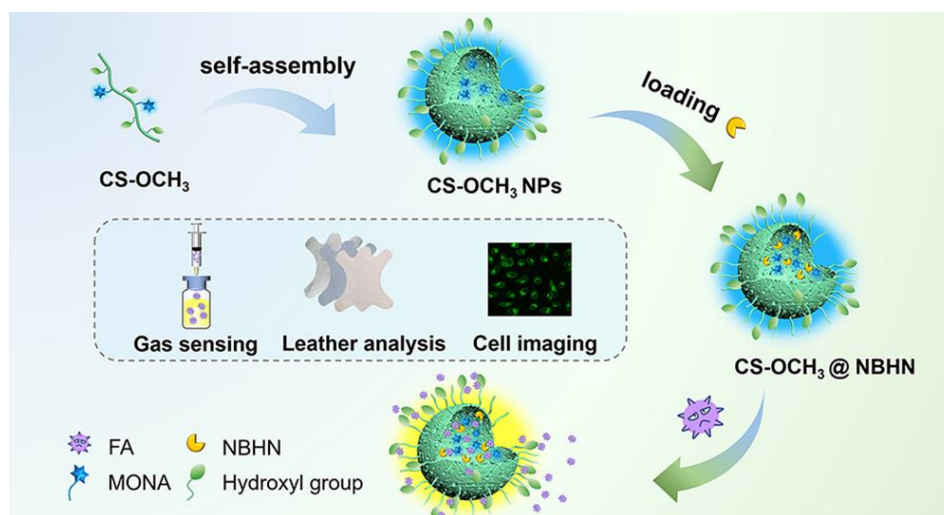


Figure 1.19 Design and Preparation of self-assembly Chitosan- based nanoparticle for FA detection.

In 2022, Kumar and co-workers⁸¹ presented a zeolite Y (DaY) with tin oxide (SnO₂) as (DaY)/SnO₂ nanoparticle- based (NP-based) sensor for lung cancer biomarkers (LCBs) detection with high selectivity and sensitivity. At various working temperatures, 200 ppb LCBs of toluene, formaldehyde, and propanol were used to assess the sensing capabilities. The sensor was discovered to be extremely effective at detecting propanol, having a great relative response and a rapid response time. The DaY/SnO₂ NP sensor had a strong relative response even at 70 ppb propanol concentrations and was stable for several detection cycles of LCBs as in **Figure 1.20**. However, this sensor cannot discriminate high molecular mass aldehydes that include aliphatic long-chain aldehydes.

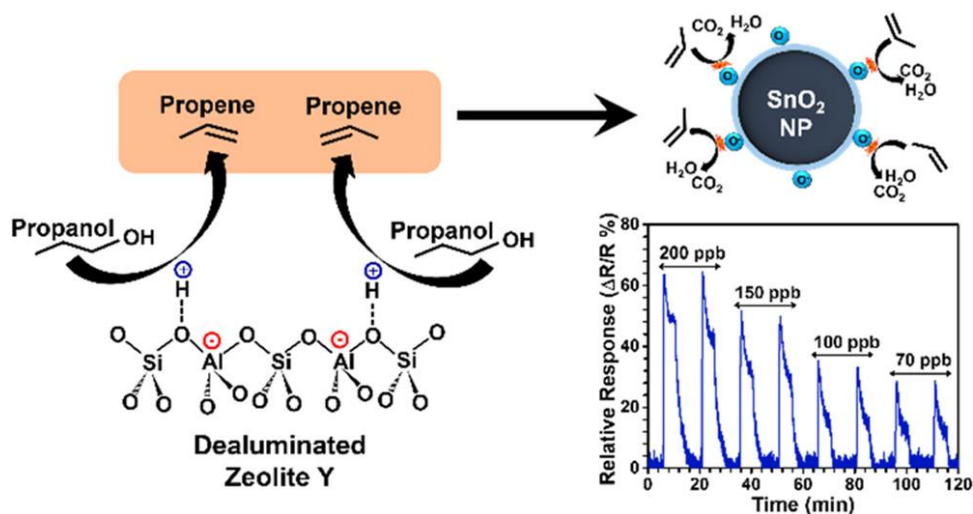


Figure 1.20 Sensing mechanism by zeolite nanoparticle.

Most of the cancer-related death worldwide is lung cancer claiming 1.59 million lives annually⁸². 84% of lung cancer reports are detected in either the later stages, typically the third or fourth, medical interventions become ineffective, and the possibility of finding a cure diminishes, because it typically remains unnoticed in the early stages. The survival rate over a five-year period experiences a significant increase, rising from 10% to 80%, when the disease is diagnosed at level 1 of growth⁸³. In the human body, free radical reactions transform cellular lipids into aldehyde molecules. The cytopathological consequences of these aldehydes include the suppression of protein and DNA synthesis. Aldehydes can serve as biomarkers indicating the presence of severe oxidative stress and atherosclerosis because of these effects⁸⁴. Most of the aldehyde detection method can only detect short chain aliphatic aldehydes, they are few research for long-chain aldehydes detection that include detection by colorimetry or vaporchromic behaviour which have several shortcomings that include colour interference with biological samples.

1.2 Research objective

- 1) To synthesize polymeric nanoparticles using naphthalimide dye-encapsulated ethyl cellulose (**EC@Naph**) as fluorescence sensors for detecting long-chain aldehyde.
- 2) To investigate the sensing capabilities of **EC@Naph** fluorescence nanosensors for the detection of long-chain aldehydes in water.

1.3 Benefit of this research

A polymeric nanosensor based on dye encapsulation for specific detection of long-chain aldehydes in water will be obtained.



CHAPTER II

EXPERIMENTAL

2.1 General procedure

2.1.1 Analytical instruments

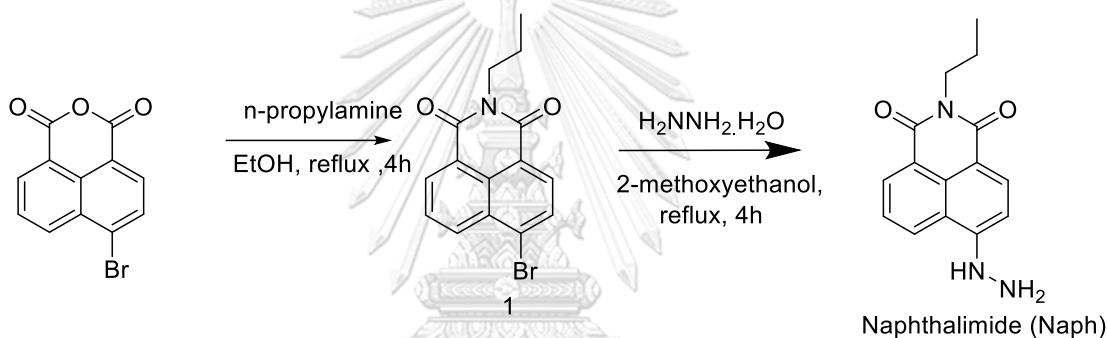
Nuclear Magnetic Resonance (NMR) spectra were collected with a Varian Mercury Plus 400 and Bruker DRX 400 MHz nuclear magnetic resonance spectrometer. Using the residual proton signal in deuterated solvents as an internal reference, chemical shifts were reported in parts per million (ppm). Using a Thermo Scientific, Nicolet 6700 FT-IR spectrometer, FT-IR spectrophotometric measurements of desiccated nanoparticle samples were obtained. Using a JEOL JEM-ARM 200F instrument with a Gantan detector and a field emission cannon with a 200 kV accelerating voltage, a SEM-EDX analysis was conducted to investigate element tomography. In addition, Mastersizer S and Zetasizer nanoseries instruments (Malvern Instrument) were used to measure hydrodynamic size and zeta potential via dynamic light scattering (DLS). Using a Varian Cary 50 Probe UV-visible Spectrometer, all UV-visible spectra were measured. All fluorescence spectra were acquired using a Varian Eclipse Probe fluorescence spectrometer and a personal computer data processing system. Cary Eclipse pulsed xenon lamp is the light source, and photomultiplier tube is the detector. Using a pH meter, the pH levels were calibrated. From the Merck Milli-Q® Reference Type 1 Water Purification System, ultrapure water was obtained.

2.1.2 Materials

The Sigma Aldrich Corporation and Fluka Corporation are the companies we purchase all the reagents and solvents required for the synthesis, Tokyo Chemical Industry (TCI) Corporation, and utilised without additional purification. According to **EC@Naph** preparation, ethyl cellulose (grade 250-300 cP; ethoxy content 48%) was acquired from Sigma-Aldrich Corporation. The reactants, including 4-bromo-1,8-naphthalic anhydride, n-propylamine, ethanol, hydrazine, and 2-methoxyethanol, were obtained from the Sigma-Aldrich Corporation. We bought aldehyde compounds including formaldehyde, propanal, butanal, pentanal, hexanal, heptanal, octanal, and nonanal from Tokyo Chemical Industry (TCI) Corporation and Sigma Aldrich Corporation for sensitivity and selectivity sensing experiments. All the reactants for

the buffer solvent, chemicals such as sodium citrate and citric acid were obtained from TCI Corporation to prepare the citrate buffer. Similarly, sodium acetate and glacial acetic acid were purchased for the acetate buffer, and sodium dihydrogen phosphate and disodium hydrogen phosphate were acquired for the phosphate buffer. The ultrapure water purification system produced MilliQ® water manufactured by Merck. In addition, the following substances were obtained from Merck: glucose (GLU), sucrose (SUC), lysine (LYS), phenylalanine (PHE), glutathione (GLUTA), urea, and NaCl as main representative compounds in plasma and the exhaled breath of individuals with lung cancer for the interference study.

2.2 Synthesis of naphthalimide dye (Naph)



Synthesis of N-propyl-4-bromo-naphthalimide (1)

4-Bromo-1,8-naphthalic anhydride 277 mg (1 mmol) was dissolved in 10 ml ethanol and the solution was heated at 80°C for 2 h. *N*-propylamine 118 mg (2 mmol) was added to the mixture of the reaction which was further refluxed for 4h. The mixture was cooled to a room temperature when the reaction was finished. The desired product, a pale-yellow solid with a yield of 72 %, was obtained when the solid was filtered, washed with cold ethanol (EtOH), and dried under vacuum.

Characterization data for *N*-propyl-4-bromo-naphthalimide (1)

¹H NMR (400 MHz, DMSO-d⁶) δ 8.54 (dd, 1H), 8.51 (dd, 1H), 8.31 (d, *J* = 8.0 Hz, 1H), 8.21 (d, *J* = 8.0 Hz, 1H), 7.97 (dd, *J*₁ = 8.3 Hz, *J*₂ = 7.5 Hz, 1H), 3.97 (t, *J* = 7.3 Hz, 2H), 1.64 (m, 2H), 0.91 (t, *J* = 7.5 Hz, 3H).

Synthesis of N-propyl-4-hydrazino-naphthalimide (Naph)

N-propyl-4-bromo-naphthalimide 64 mg (0.2 mmol) in 2.0 ml methoxyethanol was refluxed. After the solution became clear, hydrazine hydrate 1252 mg (25 mmol) was directly added into the reaction. Then, the mixed solution was refluxed for 4h. The precipitated product was filtered after reaching room temperature and rinsed with cold ethano (EtOH). In order to obtain an orange solid of a Naphthalimide derivative (Naph) with 75 % yield, recrystallization from ethanol was used to clean the crude product.

Characterization data for *N-propyl-4-hydrazino-naphthalimide (Naph)*

$^1\text{H NMR}$ (400 MHz, $\text{DMSO-}d_6$) δ 9.10 (s, 1H), 8.58 (d, $J = 8.1$ Hz, 1H), 8.42 (d, $J = 7.1$ Hz, 1H), 8.27 (d, $J = 8.7$ Hz, 1H), 7.61 (t, $J = 8.1$ Hz, 1H), 7.25 (d, $J = 8.7$ Hz, 1H), 4.64 (s, 2H), 3.94 (t, $J = 7.1$ Hz, 2H), 1.60 (m, 2H), 0.91 (t, $J = 7.5$ Hz, 3H).

2.3 Preparation of dye-encapsulated ethyl cellulose (EC@Naph) nanosensors

Utilising the anti-solvent particle induction approach, **EC@Naph** nanosensors were created in this study as described in the literature⁸⁵. To prepare a stock solution of polymeric nanosensors, 2 mg/mL of Naphthalimide dyes (**Naph**) and 1 mg/mL of ethyl cellulose (EC) were separately dissolved in acetone. According to **Table 2.1**, the amounts of EC and **Naph** in **EC@Naph** nanosensors were varied proportionally in four mg/mL ratios: 0.50:1.00, 1.00:1.00, 1.50:1.00, and 2.00:1.00. The EC solution and **Naph** solution were combined for 10 minutes at room temperature while being stirred. To create oil-in-water (o/w) nanosensors colloidal particles, 25 mL MilliQ water (anti-solvent) was added dropwise to the mixture of EC and **Naph** solution at a rate of 0.7 mL/s while being continuously stirred at 350 rpm. In this stage, the mixture transformed from a transparent yellow solution to a cloudy solution of **EC@Naph** nanomicelle. The acetone was then removed from the colloidal ethyl cellulose encapsulated **Naph** (**EC@Naph**) solution by the method of rotary evaporation. To acquire the precipitate of the as prepared **EC@Naph** nanosensors, the solution was subjected to two rounds of centrifugation at 10,000 rpm for 20 minutes each. This process effectively eliminated free Naph molecules from the supernatant. Finally, this precipitate was dispersed in 10.0 mL MilliQ water by ultrasonication for

approximately 10 minutes, and then finally collected a vial, and stored at 2-5 °C to use for a sensing application.

Table 2.1 Preparation of **EC@Naph** nanosensors by various ratios of EC and **Naph**.

Ratio of EC:Naph	Volume (μL)			Final volume (μL)
	1 mg/mL EC	Acetone	2 mg/mL Naph	
0.50:1.00	500	4000	500	5000
1.00:1.00	1000	3500	500	
1.50:1.00	1500	3000	500	
2.00:1.00	2000	2500	500	

2.4 Characterization of **EC@Naph** nanosensors

Functional groups verification of **EC@Naph** nanosensors

In order to demonstrate the constituent components and functional groups in **EC@Naph** nanosensors, Attenuated Total Reflectance-Fourier Transform Infrared Spectroscopy (ATR-FT-IR) was used to analyse **EC@Naph** nanocapsules comparing with EC and **Naph** as precursors. To obtain the **EC@Naph** precipitate, the prepared **EC@Naph** solution was then freeze-dried for 3-5 days after production.

2.4.1 Element analysis of **EC@Naph** nanosensors

Energy-dispersive X-ray spectroscopy (EDX) was combined with scanning electron microscopy (SEM) to investigate element tomography of **EC@Naph** nanoparticles. This technique is known as SEM-EDX. For sample preparation of **EC@Naph** nanoparticles for SEM-EDX, the solution of as-prepared **EC@Naph** nanosensors was freeze-dried for 2-5 days. The solid of **EC@Naph** nanosensors were scattered homogeneously on carbon tape pasted on stuff. The SEM machine was used to

acquire images and EDX mapping of **EC@Naph** nanosensors for their qualitative analysis including elements and morphology.

2.4.2 Dynamic light scattering (DLS) of EC@Naph nanosensors

Regarding the Dynamic Light Scattering (DLS) examination, the hydrodynamic dimension and polydispersity index (PDI) were analysed. In this study, 100 μL of **EC@Naph** nanosensor solution was mixed with 2,750 μL of 20 mM acetate buffer (pH 5.0). Following the addition of 100 μL nonanal (2 mM), the solution was stirred vigorously at ambient temperature for a duration of 2.0 min to ensure the completion of the complexation. Through a quartz cuvette, the hydrodynamic size and PDI values of the resulting solution of **EC@Naph** nanosensors with nonanal complexes were directly analysed. A minimum of three DLS scans were carried out at 25 $^{\circ}\text{C}$.

2.4.3 Zeta potential measurement of EC@Naph nanosensors

This work examined the zeta potential of boundary layers of nanoparticles to examine the physical stability of **EC@Naph** nanosensors. To dilute 100 μL of the as-prepared **EC@Naph** nanosensors (1:1), 2,750 μL of a 20 mM acetate buffer solution (pH 5.0) was used. After adding 100 μL , 2 mM of nonanal to the mixture, the mixture was vigorously stirred for two minutes at ambient temperature for the complexation to be completed. To measure the zeta potential values at 25 $^{\circ}\text{C}$, the complex solution of **EC@Naph** nanosensors with nonanal was introduced to pleated capillary zeta cells and measured with at least three times scans.

2.5 Optical studies of EC@Naph nanosensors

2.5.1 Fluorescence studies of the EC@Naph nanosensors

For a comprehensive examination of the optical characteristic of **EC@Naph** nanosensors, we investigated their UV-visible spectra. In this study, as-prepared **EC@Naph** nanosensors were diluted at least ten times with 2,750 μL of 20 mM acetate buffer at pH 5.0 (1:1). The **EC@Naph** nanosensors was measured by UV-visible spectroscopy. For fluorescence method, the fluorescence emission of **EC@Naph** was investigated. In this study, 100 μL of 1:1 ratio of **EC@Naph** nanosensors were diluted with 2,750 μL of 20 mM acetate buffer at pH 5.0.

Therefore, fluorescence spectroscopy was used to record the fluorescence emission spectra with settings as follows.

Start 460 nm
End 800 nm
Excitation wavelength 450 nm
PMT 650 V
Excitation slit 10.0
Emission slit 10.0.

2.5.2 Stability study of EC@Naph nanosensors

In order to examine the optical stability, the as-prepared **EC@Naph** nanosensor in aqueous solution has been placed in a vial and stored at 2-5⁰C. Under the following conditions, fluorescence signals were measured every 5 days using fluorescence spectroscopy. From the period time of 0 to 1 month, changes in emission at 550 nm of **EC@Naph** nanosensors were recorded using the above fluorescence conditions.

2.6 Selectivity studies of Naph dyes towards aldehyde families

Aldehyde molecules consisting of formaldehyde, propanal, butanal, pentanal, hexanal, heptanal, octanal, and nonanal were dissolved in spectroscopic grade dimethyl sulfoxide (DMSO) to produce a 0.06 M stock solution of aldehyde compounds. In the meanwhile, the fluorescent **Naph** dye was dissolved in acetone at 0.15 mM stock solution concentration. On the sensing experiments, a 0.15 mM stock solution of **Naph** (100 μ L) was mixed with 2.750 μ L of 20 mM acetate buffer at pH 5.0 (5 μ M) prior to the introduction of 2 mM of aldehyde guests in a final volume of 3.00 mL. At ambient temperature, the mixed solution was vigorously stirred for 2.0 min. Following the stirring procedure, fluorescence spectra were captured using fluorescence spectroscopy with predetermined conditions outlined below.

Start 460 nm
 End 800 nm
 Excitation wavelength 455 nm
 PMT 600 V
 Excitation slit 5.0
 Emission slit 5.0

2.7 Optimisation of the EC@Naph nanosensors for long-chain aldehydes detection

2.7.1 pH investigations of EC@Naph nanosensors in micellar platforms for nonanal detection

To investigate the impact of pH on the detection system, 100 μL of the as-prepared **EC@Naph** nanosensor solution was mixed with 2,750 μL of various 20 mM buffer solutions with varying pH, as shown in **Table 2.2**. In addition, 0.06 M stock solution of nonanal was then added at a concentration of 0 μM as a blank and 2 mM into the corresponding solution and adjusted to 3.00 mL final volume with dimethyl sulfoxide (DMSO) spectroscopic grade. At ambient temperature, the resulting solution was vigorously stirred for 2.0 min to complete the complexation. With respect to the above conditions, the fluorescence spectra of **EC@Naph** nanosensors were captured with and without nonanal in various pH buffers.

Table 2.2 The variation in buffer at various pH levels.

pH	Buffer
3.0	Citric buffer 0.02 M
4.0 and 5.0	Acetate buffer 0.02 M
6.0, 7.0, 7.4 and 8.0	Phosphate buffer 0.02 M

2.8 Selectivity test of EC@Naph nanosensors towards detection of various aldehyde compounds

The 0.06 M stock solutions of the aldehyde family were made in spectroscopic grade dimethyl sulfoxide (DMSO), the preparations detailed are outline in **Table 2.3**.

Table 2.3 The preparation of 0.06 M stock solution of aldehyde family as guests at 10.00 mL.

Guests	Molecular weight (g/mol)	Density (mg/mL)	Weight (mg)	Volume (μ L)
Formaldehyde (C1)	30.03	1.10	18.00	16.36
Propanal (C3)	58.08	0.81	34.85	42.96
Butanal (C4)	72.11	0.80	43.27	54.13
Pentanal (C5)	86.13	0.81	51.68	63.80
Hexanal (C6)	100.16	0.81	60.10	74.19
Heptanal (C7)	114.18	0.81	68.51	84.58
Octanal (C8)	128.21	0.82	76.93	94.97
Nonanal (C9)	142.24	0.83	85.34	102.82

In the beginning of this investigation, representative guests were examined at a final concentration of 2 mM. The 0.06 M guest solution was subsequently diluted to give the 2 mM of the aldehyde guests that includes formaldehyde, propanal, butanal, pentanal, hexanal, heptanal, octanal, and nonanal (**Table 2.3**). As a test of the selectiveness of our system, 100 μ L of each ratio from stock solution of as-prepared **EC@Naph** nanosensors was mixed with 2,750 μ L of 20 mM acetate buffer, pH 5.0. After adding 2 mM of aldehyde molecules (**Table 2.3**) to the solution, the resulted mixture was then vigorously stirred at 2 minutes reaction time to complete the complexation. The fluorescence emission was recorded under the same conditions listed in **Table 2.4**.

Table 2.4 Fluorescence settings for measuring selectivity for all **EC@Naph** nanosensor prepared in various ratios.

Ratio of EC:Naph	0.50:1.00	1.00:1.00	1.50:1.00	2.00:1.00
Start (nm)	460			
End (nm)	800			
Excitation wavelength (nm)	450			
Excitation slit	5.0			
Emission slit	5.0			
PMT (V)	550			

In addition to naked-eye detection, 100 μL of as-prepared **EC@Naph** nanosensors solution prepared by 1:1 was mixed with 2,750 μL acetate buffer (20 mM, pH 5.0). In addition, 2 mM of the aldehyde guest that includes formaldehyde, propanal, butanal, pentanal, hexanal, heptanal, octanal, and nonanal, was added to the corresponding solution to make a final volume of 3.0 mL followed by stirring vigorously at ambient temperature for two minutes to complete the complexation. Fluorescence brightness of **EC@Naph** nanosensors was monitored using UV irradiation at 365 nm.

2.9 Quantitative analysis of **EC@Naph** nanosensors for nonanal detection

By means of fluorescence titration experiments, the lowest concentration of quantitative analysis of 1:1 ratio of EC and **Naph** for **EC@Naph** preparation towards nonanal as long-chain aldehyde sensing was determined. As shown in **Table 2.5**, a stock solution of 10 mM nonanal guest was prepared in spectroscopic grade dimethyl sulfoxide (DMSO).

Table 2.5 The preparation of nonanal compound at a 10 mM concentration in 10.00 mL.

Aldehyde	Molecular weight (g/mol)	Density (mg/mL)	Weight (mg)	Volume (μ L)
Nonanal (C9)	142.24	0.83	14.22	17.14

In accordance with **Table 2.6**, different nonanal concentrations as the target molecules were added to 2,750 μ L of 20 mM acetate buffer pH 5.0 in 100 μ L of the as-prepared **EC@Naph** nanosensor solution prepared by 1:1 ratio. The resulting mixture was adjusted to 3.0 mL volume with DMSO and stirred at ambient temperature for 2.0 min. The fluorescence responds were then captured using the settings listed in **Table 2.7**. I and I_0 represented the fluorescence emission intensities of **EC@Naph** nanosensors with and without nonanal respectively at the maximum wavelength of \sim 550 nm. In this study, the correlation between nonanal concentration and relative fluorescence intensity ($I-I_0$) was used to construct the standard calibration curve.

Table 2.6 The concentration of nonanal in **EC@Naph** nanosensors system.

Entry	Stock [aldehyde] (mM)	Equivalent of nonanal guest molecule	Final volume [Nonanal] added in 3 mL final (μM)	V aldehyde (μL)	V DMSO (μL)
Blank	0	0	0	0	150.0
1.	10	5	25	7.5	142.5
2.		10	50	15	135
3.		15	75	22.5	127.5
4.		20	100	30	120
5.		30	150	45	105
6.		40	200	60	90
7.		50	250	75	75
8.		60	300	90	60
9.		70	350	105	45
10.		80	400	120	30
11.		85	425	127.5	22.5
12.		90	450	135	15
13		95	475	142.5	7.5
14.		100	500	150	0

Table 2.7 Conditions for the fluorescence of **EC@Naph** nanosensors made with a 1:1 mixture of EC and **Naph** in an aqueous media for a quantification study of nonanal detection.

Conditions	EC@Naph with nonanal (C9)
Start (nm)	460
End (nm)	800
Excitation wavelength (nm)	450
PMT (V)	750
Excitation slit	5.0
Emission slit	5.0

2.10 Quantitative investigation of EC@Naph with nonanal by visual detection

In this study, the nonanal detecting ability of **EC@Naph** nanosensors made by combining EC and **Naph** in a ratio of 1:1 was quantified using naked-eye detection. 100 μL of the as-prepared **EC@Naph** nanosensor solution was mixed with 2,750 μL of 20 mM acetate buffer pH 5.0. Next, various concentrations of nonanal ranging from 0.00 μM to 1.50 mM were added into the aforementioned solution followed by rapid stirring at ambient temperature for 2.0 min to complete the complexation. Under UV light of 365 nm, the fluorescence brightness of **EC@Naph** nanosensors with various concentrations of nonanal was analysed to determine the lowest concentration of nonanal detection with the naked eye.

2.11 Interference studies of EC@Naph nanosensors

As shown in **Table 2.8**, stock solutions of aldehyde compounds, such as formaldehyde (FA), propanal (PRO), and benzaldehyde (BA), and also significant representative compounds in blood and exhaled breath of individuals having lung cancer were made at a concentration of 20 mM in dimethyl sulfoxide (DMSO) spectroscopic grade using 20 mM acetate buffer pH 5.0.

Table 2.8 The preparation of a 10.00 mL final volume 20 mM stock solution of aldehyde and a crucial representative components in blood and exhaled breath.

Guests	Solvents	Molecular weight (g/mol)	Weight (mg)
Formaldehyde (FA)	DMSO	30.03	6.01
Propanal (PRO)	DMSO	58.08	11.60
Benzaldehyde (BA)	DMSO	106.12	21.20
Nonanal	DMSO	142.24	28.40
Glucose (GLU)	20 mM acetate buffer pH 5.0	180.16	36.00
Sucrose (SUC)	20 mM acetate buffer pH 5.0	342.3	68.46
Lysine (LYS)	20 mM acetate buffer pH 5.0	146.19	29.24
Phenylalanine (PHE)	20 mM acetate buffer pH 5.0	165.19	33.04
Glutathione (GLUTA)	20 mM acetate buffer pH 5.0	307.3	61.46
Urea	20 mM acetate buffer pH 5.0	60.06	12.00
NaCl	20 mM acetate buffer pH 5.0	58.44	11.69

Each component of the sensing system for interference investigation in this experiment contained 100 mL of EC@Naph nanosensors, 500 mM nonanal solution, and 500 mM additional interfering substances, as main plasma and exhale breath compounds (glucose, sucrose, lysine, phenylalanine, glutathione, urea, and NaCl in 20 mM acetate buffer pH 5.0) or aldehyde families such as formaldehyde, propanal and benzaldehyde in DMSO spectroscopic grade. In terms of preparing each component for interference investigations, 100 μ L of **EC@Naph** nanosensor solution and A final volume of 3.00 mL was obtained by mixing 75 μ L of 20 mM nonanal in DMSO with 75 μ L of 20 mM additional interferences and 2,750 μ L of 20 mM acetate buffer, pH 5.0. The resulting solution was then vigorously stirred at room temperature for two minutes for complete complexation before measuring fluorescence responses. Under

the above fluorescence spectroscopy conditions, the fluorescence responds were captured. To facilitate comprehension, bar graphs of emission at 550 nm based on both the presence and absence of interference guests, the relative fluorescence intensities ($I-I_0$) of **EC@Naph** nanosensors with nonanal were determined. I_0 and I were assigned to before and after the introduction of organic guests to **EC@Naph** nanosensors respectively.



CHAPTER III

RESULT AND DISCUSSION

3.1 Design Concept of Naphthalimide encapsulated sensors for Long-Chain Aldehydes detection

Owing to their optical stability, larger Stokes shifts, a higher quantum yield, and a significant environmental influence on their emission and absorption, naphthalimide has attracted the scientific community's interest as optical sensors⁸⁶⁻⁹⁵. Nevertheless, As a versatile chemical, naphthalimide is commonly employed fluorophore unit⁹⁶. Naphthalimide-based hydrazine is a great platform to facilitate the design of fluorescent probes for general aldehyde detection⁶⁸. At ambient temperature, the naphthalimide contains a nucleophilic hydrazine which readily condenses with aldehydes creating stable fluorescent compounds. The hydrazine group, which is responsible for the photo-induced electron transfer (PET) behaviour, is inhibited when it condenses with aldehydes due to its considerable capability for electron donation and however resulting in fluorescence enhancement.

It is extremely likely that long-chain aldehydes that includes hexanal, heptanal, octanal, and nonanal identified in tumour tissue, blood, urine, and exhaled breath are among the lung cancer biomarkers^{97, 98}. The concentrations of lung-chain aldehydes were observed to be considerably greater in individuals with lung cancer compared to control group.⁹⁹ Therefore, one of the most obvious signs of lung cancer is the high level of these long-chain aldehyde families. Moreover, Long-chain aldehydes have two parts in their chemical structure: a functional group that is reactive to hydrazine via Schiff base reaction or imine bond formation and a hydrophobic aliphatic chain.

As shown in **Figure 3.1(a)** naphthalimide-based hydrazine (**Naph**) was used as a fluorophore for detection of long-chain aldehyde compounds in this study. The **Naph** can produce an imine bond through a covalent reaction with carbonyl aldehyde. Due to insolubility of **Naph** in water, the natural ethyl cellulose (EC) polymer in **Figure 3.1(b)** was chosen as an excellent choice to encapsulate **Naph** to increase its water solubility. By stirring EC and **Naph** in acetone to mix them together, thereby, they created hydrogen bonds and hydrophobic interactions in order to physically

adsorb substances. Subsequently, the self-assembly polymeric micelle was likely produced by the constant dropping of water (antisolvent) to create **EC@Naph** nanoparticles. The hydrophilic hydroxyl site was made to face away from the polar aqueous environment by EC, as seen by the gradual transformation of the micelle-like nanoparticles into yellow colloidal nanoparticles. In the interim, adsorptions via hydrogen-bonding and the remaining ethyl ether alternatives interacted hydrophobically with the dye to create self-assembling dye-encapsulating nanoparticles. The optimum EC to **Naph** dye ratio yielded **EC@Naph** nanosensors with loosen encapsulation and a poor fluorescence signal. To create the fully enclosed tight nanoparticles and enable the fluorescence intensification of dye-encapsulation, the hydrophobic interactions and imine bond formation of **Naph** encapsulated in EC polymer with an aldehyde group as a guest molecule were crucial driving forces (**Scheme 3.1**).

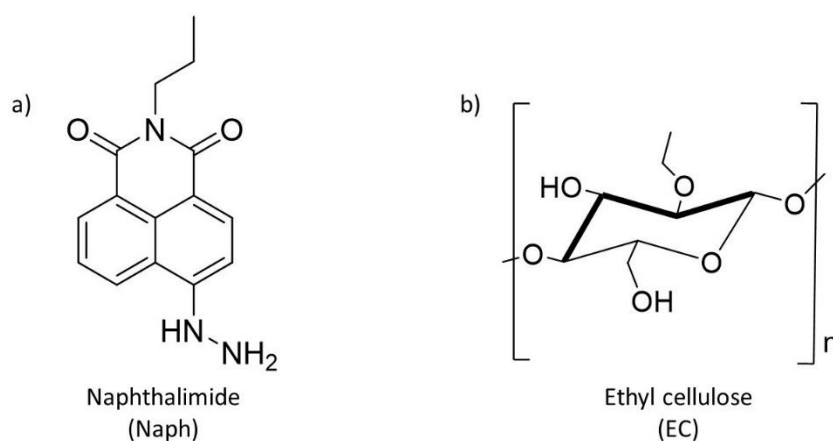
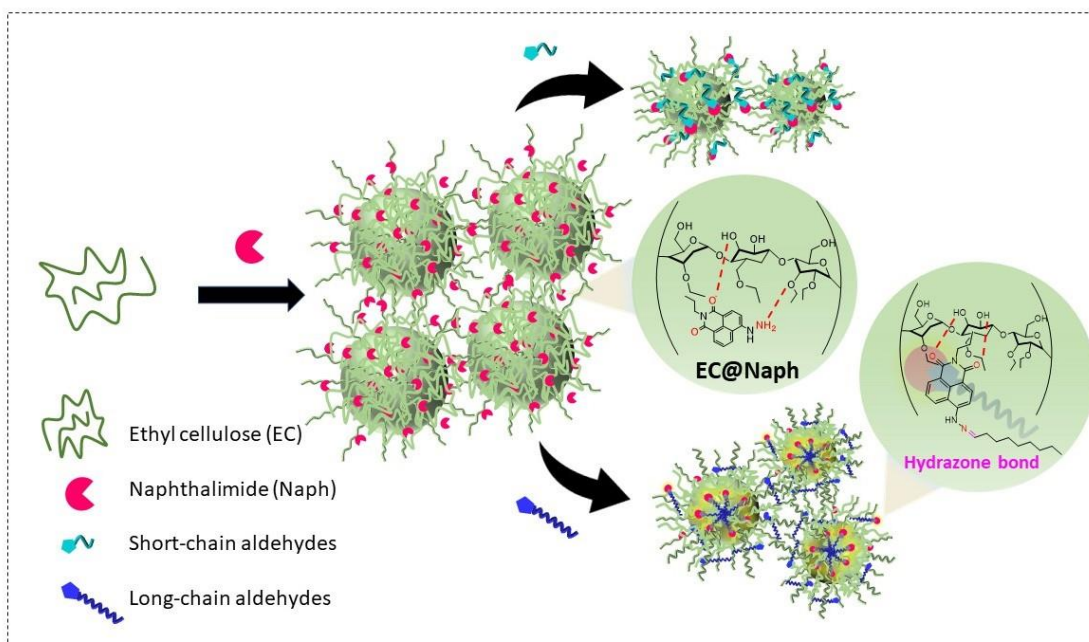


Figure 3.1 Structures of Naphthalimide-based hydrazine (**Naph**) a) and Ethyl cellulose polymer (EC) b)21.



Scheme 3.1. Conceptual design of the **EC@Naph** sensing platform for the detection of long-chain aldehydes²².

3.2 Synthesis and characterization of Naphthalimide (Naph)

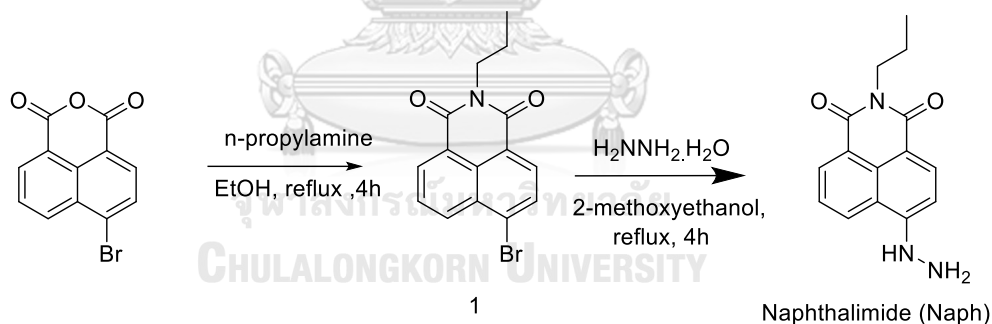


Figure 3.2 Synthesis of Naphthalimide dye (**Naph**)²³.

Naph was successfully synthesized in two step reactions (**Figure 3.2**). As an initial step, 4-bromo-1,8-naphthalic anhydride was reacted with *n*-propylamine in ethanol (EtOH) for an appropriate time to give intermediate 1. Moreover, In the next step, compound 1 was reacted with hydrazine via a process of aromatic substitution with nucleophiles. By utilising 2-methoxyethanol as a solvent, the nitrogen atom's nucleophilic lone pair electron in hydrazine would replace the bromo atom in compound 1 to afford **Naph** as orange yellow in 72% yield. The completion of

reactions was monitor by thin-layer chromatography (TLC) on silica gel using 5% Ethyl acetate (EtOA): dichloromethane (DCM) as eluent ¹⁰⁰. From the ¹H-NMR data of compound **1** in **Figure 3.3**, the signals at 0.92, 1.65 and 3.99 ppm are assigned to propylamine proton peaks attached to the aromatic naphthalimide unit by nucleophilic substitution. The ¹H-NMR spectrum of naphthalimide dye (**Naph**) in **Figure 3.4** showed a signals of NH hydrazine group at 3.96 and 4.66 ppm. These peaks' existence supports compound **1** and naphthalimide dye were formed (**Naph**).

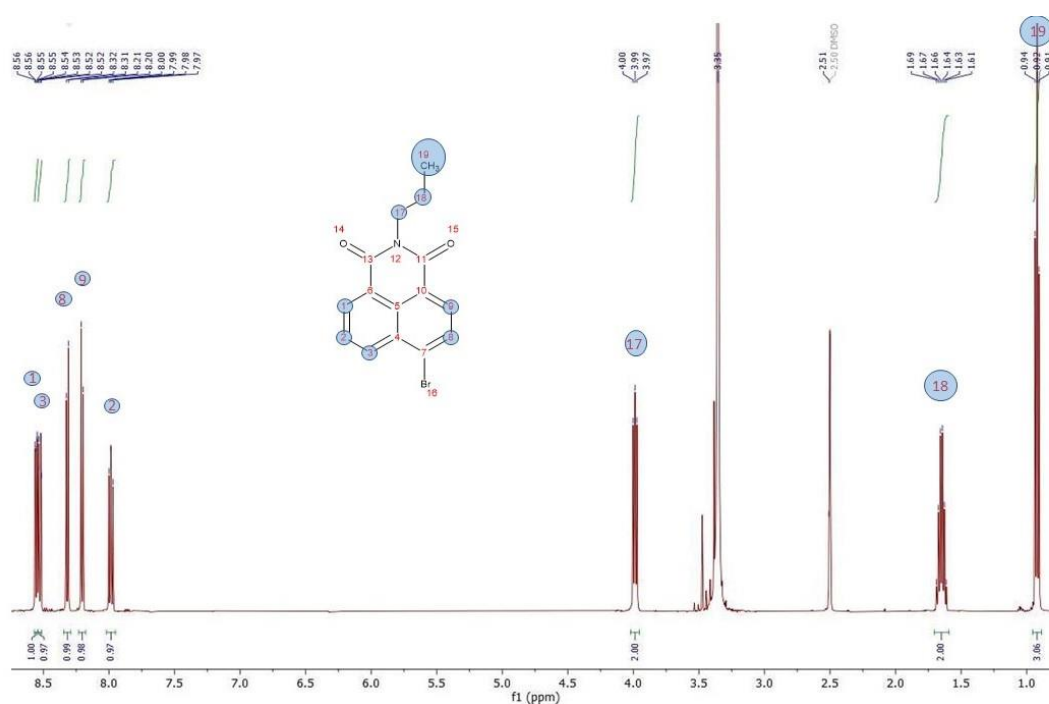


Figure 3.3 ¹H NMR spectrum of compound 124.

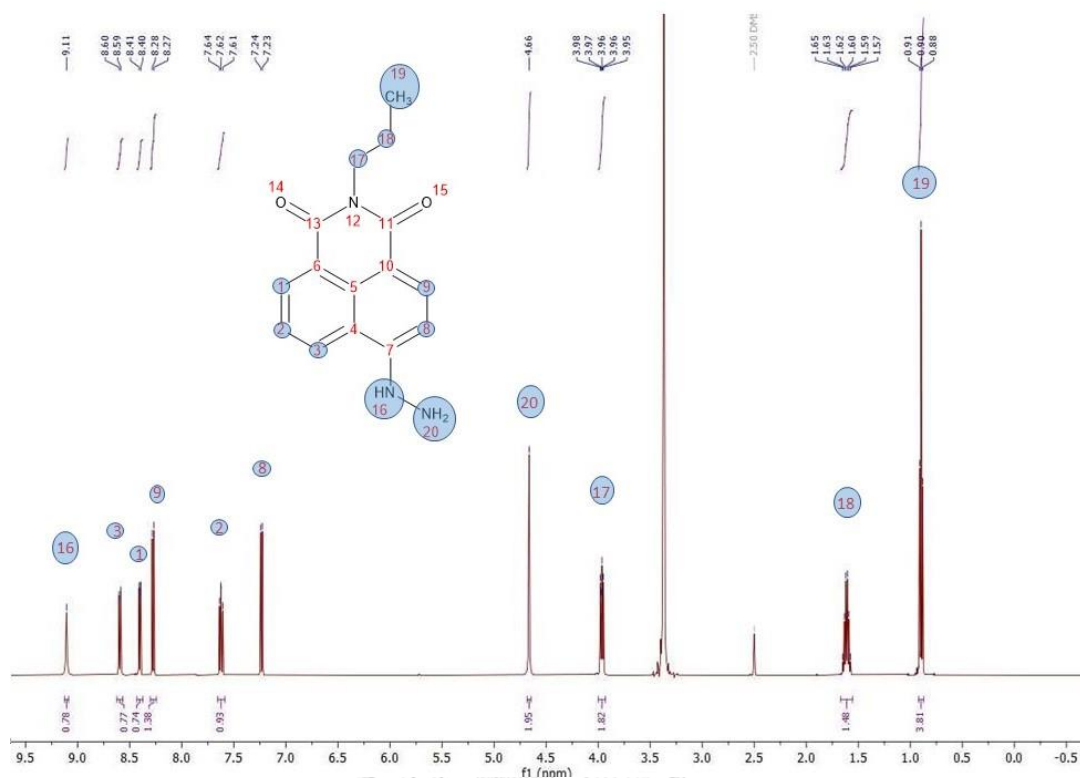


Figure 3.4 ¹H NMR spectrum of Naphthalimide dye (**Naph**)25.

3.3 Preparation of fluorescence dye-encapsulated by ethyl cellulose nanosensors

The antisolvent particle induction approach was used to create ethyl cellulose nanosensors with dye encapsulation (**EC@Naph**). To increase the **Naph**'s solubility in water, the natural ethyl cellulose (EC) polymer was selected as an effective choice for encapsulation. Physical adsorptions were produced throughout the encapsulation process by EC backbones being mixed and stirred in acetone producing hydrogen-bonding and hydrophobic interactions. Following the creation of the self-assembling polymeric nanomicelle, the **EC@Naph** nanoparticles were probably produced through constant water dropping (an antisolvent). The micellar-like nanoparticles changed gradually into colloidal nanoparticles. This may be as a result of the hydrophilic hydroxyl site pointed to the aqueous polar environment. As a result of hydrophobic interactions with the dye, the residual ethyl ether substitutes self-assembled into dye-encapsulating nanoparticles. The **EC@Naph** nanosensors with the optimised EC to dye ratio had a weaker fluorescence signal because of loose

encapsulation. The inherent Important driving factors in the development of the fully enclosed tight nanoparticles included hydrophobic interactions and imine production of **Naph** encapsulated in EC with an aldehyde group as the target molecules that result in promoting the fluorescent signal of dye-encapsulation after making complex to the long-chain aldehydes (**Figure 3.5**).

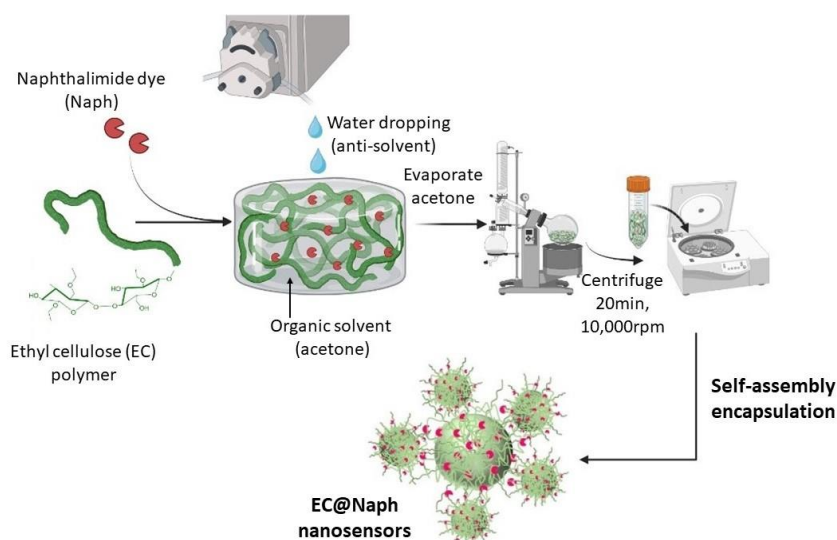


Figure 3.5 Design of **EC@Naph** nanosensor with respect to long-chain aldehydes detection²⁶.

3.4 Characterization of **Naph** encapsulated by ethyl cellulose (**EC@Naph**)

3.4.1 Fourier transform infrared spectroscopy (FT-IR)

The functional groups on the **EC@Naph** structure were examined by Attenuated Total Reflectance-Fourier Transform Infrared spectroscopy (ATR-FTIR) to elucidate the capability of **Naph** dye to bind physically with ethyl cellulose (EC). The component structures of ethyl cellulose (EC) and naphthalimide dye (**Naph**) as precursors and the **EC@Naph** nanosensors contained comparable functional groups. In relation to FT-IR measurement (**Figure 3.6**), the OH group, the CH₂ group of cellulose, and the COC stretching vibration of the ethoxy group, respectively, are represented by separate peaks in the EC powder absorption spectra at around 3350, 2970-2865, and 1060 cm⁻¹. The aliphatic primary NH stretching of the hydrazide group at 3300 cm⁻¹, the carbonyl peak at 1750 cm⁻¹, and the peak at roughly 1645 cm⁻¹

due to the carbonyl amide groups were all seen in the FT-IR spectra of **Naph** dye. Most characteristic peaks of the **Naph** structure settled in a difficult-to-identified fingerprint region. As demonstrated by the FT-IR spectrum of **EC@Naph** nanomaterials, it was clear that EC and **Naph** important characteristic peaks mixed together. The result demonstrated that **Naph** dye could physical adsorption onto the polymeric EC backbone which was accomplished through the encapsulation process.

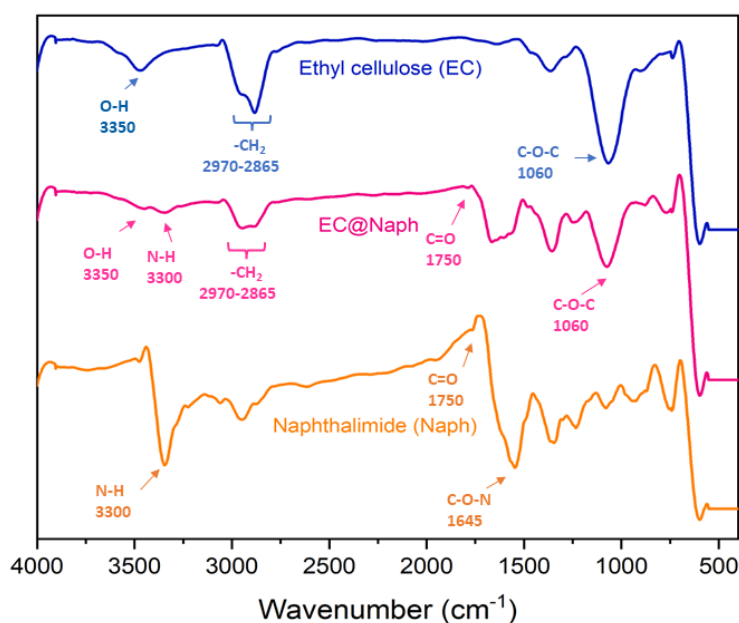


Figure 3.6 ATR-FTIR spectra of ethyl cellulose (EC, blue), **EC@Naph** nanosensor (Magenta) and that of Naphthalimide dye (**Naph**, orange)²⁷.

3.4.2 Scanning electron microscopy coupled energy dispersive x-ray spectroscopy (SEM-EDX)

In addition, the elemental composition of the nanosensor was analysed using SEM-EDX, which revealed the presence of Nitrogen (N) atom, Oxygen (O) atom, and Carbon (C) atom. This indicates **Naph** dye encapsulation by EC (**Figure 3.7**). According to the findings, the EDX maps revealed that **EC@Naph** nanosensors detected C, N, and O elements dispersed with the particles. Moreover **Figure 3.8** shows the percentage composition of carbon (C), Oxygen (O) and nitrogen (N). Consequently, it was evident that hydrazine-functionalized **Naph** dye was encapsulated in the EC polymer backbone. In addition, this demonstrated that water-

insoluble **Naph** dye coexisted favourably at the hydrophobic core of **EC@Naph** nanoparticles, supporting our hypothesis that **Naph** is enclosed within the EC backbone.

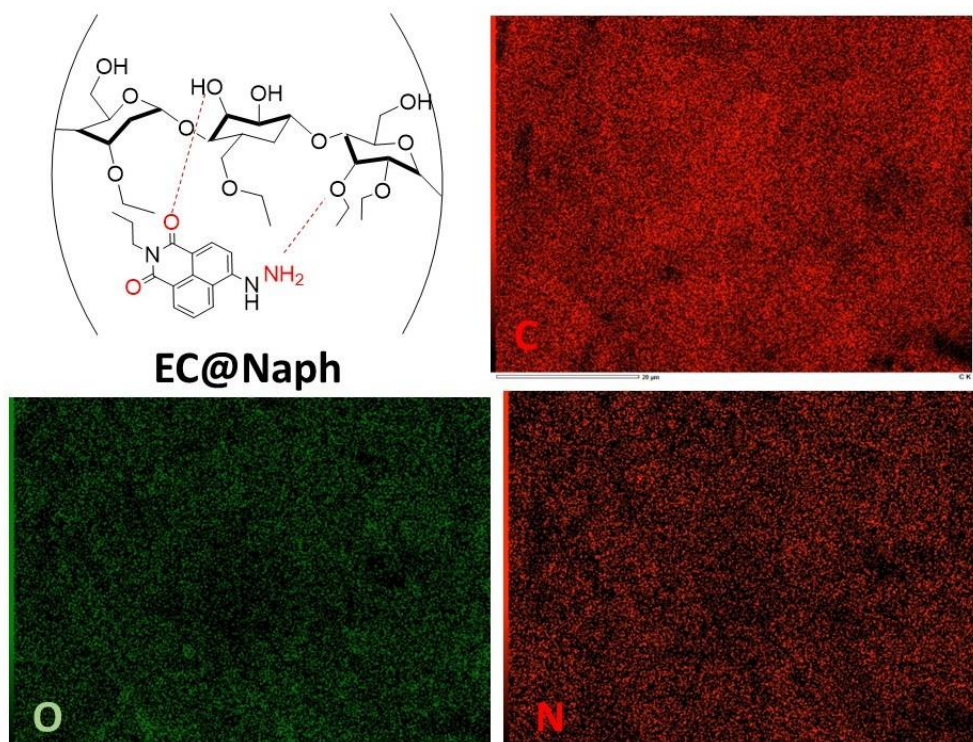


Figure 3.7 SEM-EDX map of **EC@Naph** nanosensor28.

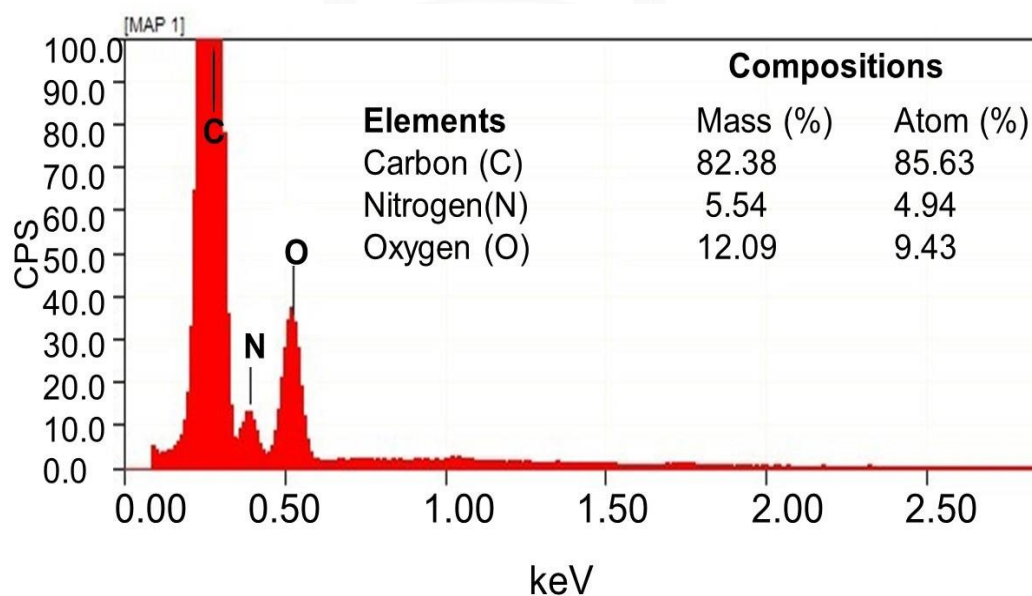


Figure 3.8 EDX Spectrum of **EC@Naph**29.

3.4.3 Optical property study of EC@Naph nanosensor

Utilising UV-visible and fluorescence spectroscopy, optical properties of **EC@Naph** nanosensor in aqueous media were investigated. The UV visible spectrum of **EC@Naph** nanosensors (red line) has the absorbance max at 450 nm. Fluorescence emission spectrum of **EC@Naph** (black line) has a peak at 550 nm. The insert is UV-visible (yellow) and fluorescence images of **EC@Naph** under UV lamp irradiation at 365nm. The **EC@Naph** showed weak fluorescence under UV lamp irradiation, this is due to the loosen encapsulation of **EC@Naph** nanosensors that result in weak fluorescence.

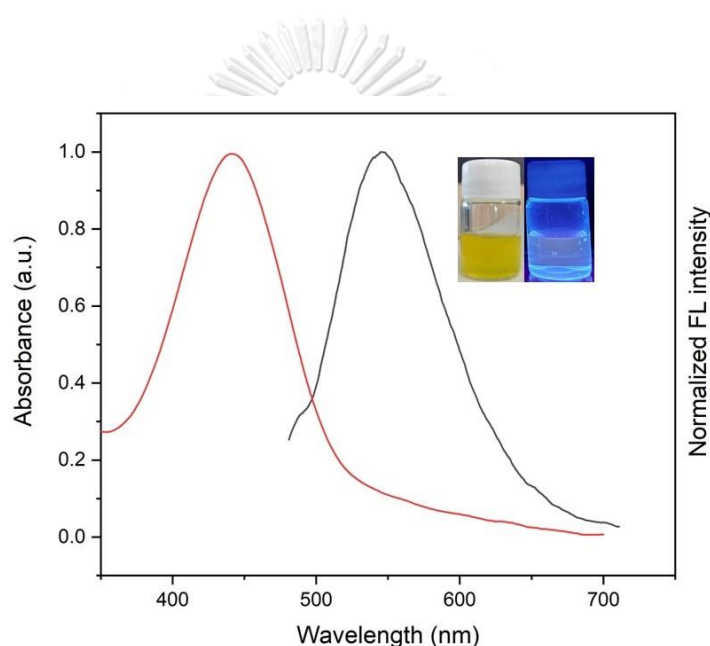


Figure 3.9 Absorbance (Abs) left, and fluorescence emission (Em) intensities right of **EC@Naph** nanosensors in aqueous media³⁰.

3.5 The stability study of EC@Naph nanosensors

For a period of one month, the fluorescence intensities of **EC@Naph** nanosensor in aqueous media at 2-5⁰C were measured at various times using fluorescence spectroscopy to determine its stability. **Figure 3.10** demonstrates that the fluorescence intensity of **EC@Naph** remained constant which indicates that the **EC@Naph** nanosensors fluorescence properties are stable in aqueous solution. It reveals that **EC@Naph** has not undergone any significant decomposition. Due to these remarkable properties, the synthesized **EC@Naph** nanosensor is a desirable

nanomaterial for sensing applications. Furthermore, the decomposition of the sensing platform reduces the amount of **Naph** encapsulated in EC backbone, however, this result in incomplete encapsulation of **Naph**. This event led to larger colloidal particles becoming suspended in water as a result. The eventual precipitation of the solution had an impact on the fluorescence intensities of **EC@Naph** nanosensors.

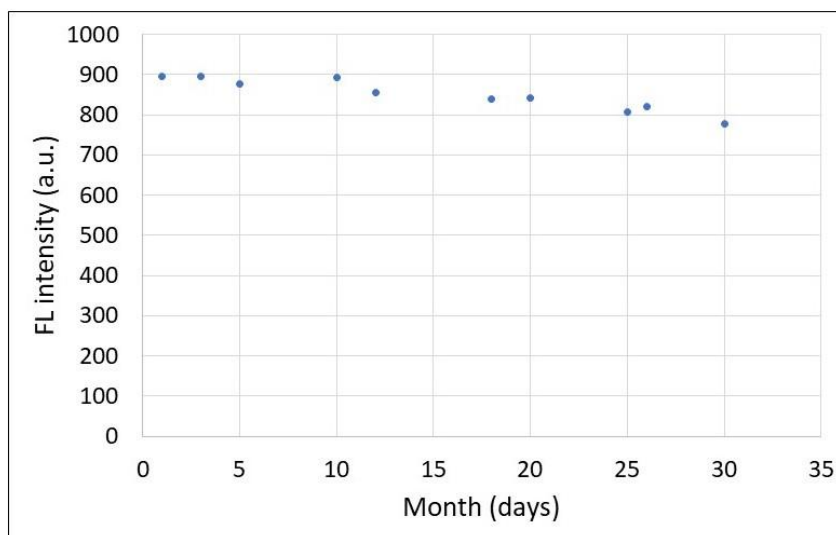


Figure 3.10 A Plot showing the stability of **EC@Naph** nanoparticle at $\lambda_{em} = 550$ nm over 1 month at 2-5°C ($\lambda_{ex} = 450$ nm, PMT 650 V, slit 10nm)³¹.

3.6 Dynamic light scattering (DLS) and zeta potential studies

To assess hydrodynamic diameters, DLS measurements were carried out (**Figure 3.11**). With nonanal at reaction time of 2.0 minutes, the uniform particle sizes of **EC@Naph** nanosensors decrease, which indicated that nonanal effectively bound with **EC@Naph** inducing the tight encapsulation of nanoparticle. **EC@Naph** nanosensors prepared by combining EC and **Naph** dye in various ratios that include 0.5:1.0, 1.0:1.0, 1.5:1.0 and 2.0:1.0 with intensity difference between octanal and nonanal as 226 a.u, 270 a.u, 39 a.u and 131 a.u respectively. The 1.0:1.0 ratio displaying the greatest intensity differences is indicative of the properly fitting creation of micellar **EC@Naph** nanosensors. As a result, the fluorescence signal of **EC@Naph** nanosensors may be improved by the optimal encapsulation of the micelle formation. This indicated that **EC@Naph** prepared with a 1:1 ratio detected nonanal as a long-chain aldehyde guest with a high sensitivity, according to our concept.

Long-chain aldehydes was able to easily go through nanoparticles' cores and bond chemically with the fluorescent compound based on hydrazine units owing to the loose encapsulation behaviour of sensing nanomaterials. As a result, they showed that **EC@Naph** nanosensors produced with a 1:1 ratio of EC and **Naph** are capable of detecting nonanal in aqueous solutions. The polydispersity index (PDI) was investigated to evaluate the consistency of the particle size distribution^{101, 102}. In general, the smaller PDI values corresponded to a more uniform particulate size distribution^{103, 104}. As shown in **Table 3.1**, according to the data, the PDI values of **EC@Naph** with nonanal (C9) indicated a moderately polydispersed particle size distribution. Additionally, the polymeric nanoparticles' outer surfaces were capable of adsorbing the acetate buffer, as shown by the zeta potential measurements, which represent the surface charges present in the boundary layers of nanoparticles immersed in aqueous environment¹⁰⁵⁻¹⁰⁷. Based on the basic principle of zeta potential values, when the zeta potential lowers below -30 mV, it implies a very stable physical state. The significant negative zeta potential value of -50.9 mV in the case of **EC@Naph** nanosensors complexed with nonanal denotes outstanding physical stability. This is attributed to the electrostatic repulsions between the individual particles (**Figure 3.12**). Moreover, the polar functional group on nonanal may be adsorbed on the surface of the **EC@Naph**, this adsorption result in enhancement of surface's negative charge of the system (**Figure 3.12**).

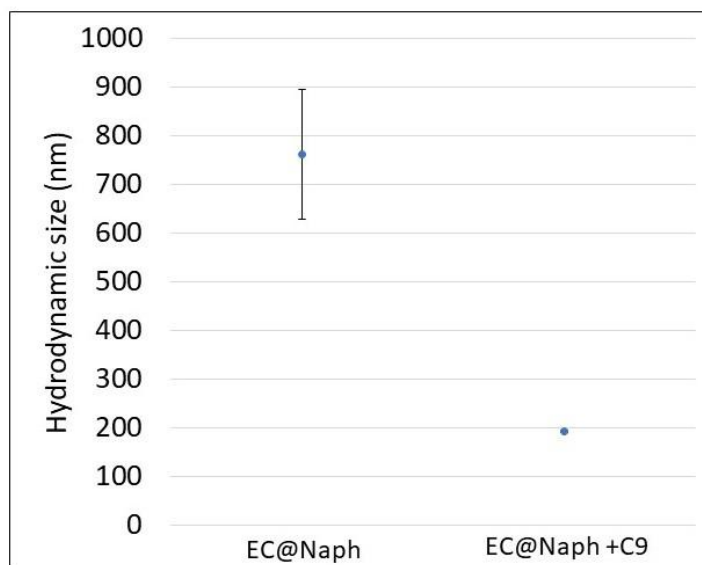


Figure 3.11 Dynamic light scattering (DLS) measurement of **EC@Naph** without and with nonanal (C9)32.

Table 3.1 Hydrodynamic diameter of particle, polydispersity index (PDI) and zeta potential measurement of **EC@Naph** nanosensors with and without nonanal (C9) guest molecule9.

Component	Size (nm)	PDI	Zetapotential (mV)
EC@Naph	762.3 ± 133.7	0.807±0.04	-29.3±1.05
EC@Naph+ C9	192.4 ± 2.11	0.138±0.03	-50.9±1.37

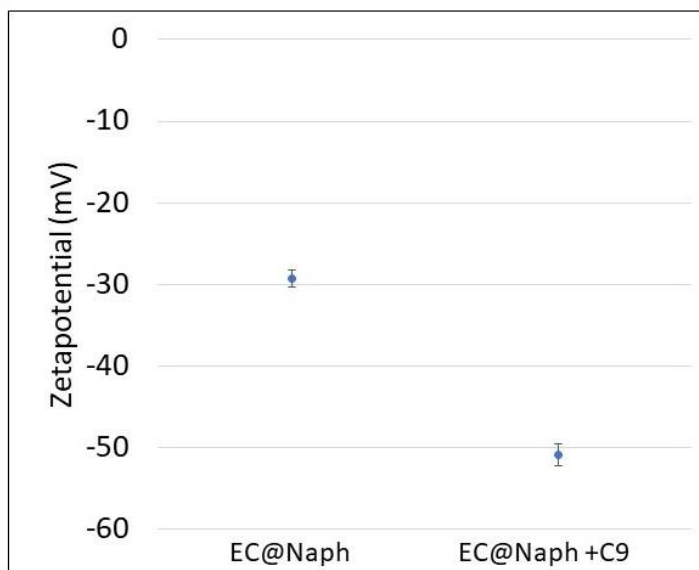


Figure 3.12 Zeta potential measurement of **EC@Naph** with and without nonanal (C9)33.

3.7 Investigation into the reaction time of EC@Naph with nonanal

To examine the reaction time between **EC@Naph** and nonanal, fluorescence responses were measured at different time intervals ranging from 1 to 10 minutes. These measurements were conducted in a 20 mM acetate buffer with a pH of 5.0 (**Figure 3.13**). The fluorescence spectra show gradual fluorescence quenching as the reaction time increases. The reaction time of 2.0 minutes between **EC@Naph** and nonanal was selected for further investigations due to its optimal time for generating the maximum fluorescence intensity. The observation of the decrease in fluorescence intensity as reaction time increase was possibly caused by the solubility. After the reaction of naphthalimide and nonanal, naphthalimide's solubility or dispersibility inside the ethyl cellulose matrix was changed. The precipitate of hydrazone naphthalimide product upon the longer reaction time was occurred causing the fluorescence quenching.

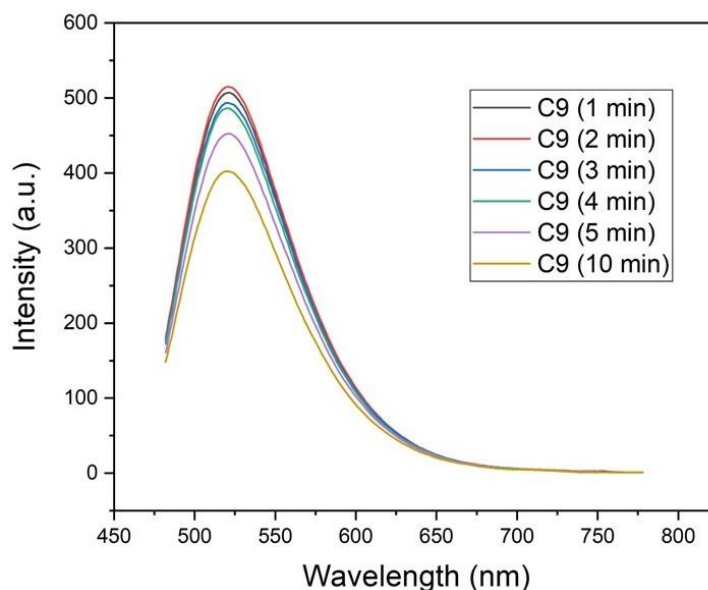


Figure 3.13 Reaction time variation of **EC@Naph** nanosensors with nonanal (C9) (2mM stock in DMSO) guest molecule³⁴.

3.8 Sensing properties of **EC@Naph** towards nonanal

After establishing the vital sensing functions of hydrazine-functionalized fluorescence dyes, the selectivity of **Naph** for aldehyde family detection was investigated as a challenge for sensory platforms. The aldehydes considered in this study can be categorized into two classes with respect to their alkyl chain length. The first group comprises aldehydes with short-chain alkyl groups, including formaldehyde, propanal, butanal, and pentanal. The second group consists of aldehydes with long-chain alkyl groups, namely hexanal, heptanal, octanal, and nonanal) were employed as representative target molecules (guest). After 2.0 minutes of stirring, the fluorescence spectrum of the mixture solution was recorded using excitation wavelength of 450 nm after these target molecules were added. As depicted in **Figure 3.14** (a), in the presence of various aldehyde families, the emission signals of **Naph** were observed at a lower wavelength (blue shift) than **Naph** in the absence of long-chain aldehydes. The fact that this fluorophore, **Naph**, reacted admirably with all aldehyde compounds to produce imine bond via Schiff-base reaction is indicative of its excellent reactivity as in **Figure 3.14**. In contrast, the fluorophore **Naph** showed weak selectivity for aldehydes detection, as demonstrated by this experiment's conclusive findings and from the visual images in **Figure 3.15** (b). According to the

proposal, it was established that the sensing system utilized in this study necessitated the utilization of natural ethyl cellulose polymer (EC). This choice served the dual purpose of improving the water solubility of **Naph** for sensing applications and significantly enhancing the selective detection of long-chain aldehydes. Due to its small size and relative rigidity, formaldehyde is less likely to aggregate or experience intermolecular interactions that could quench fluorescence. This allows for better interaction between the molecule's excitation state and its environment, increasing fluorescence efficiency as shown in **Figure 3.15a** and higher fluorescence brightness as shown in **Figure 3.15b** whereas long-chain aldehydes with their longer and more flexible structures are more likely to show intermolecular interactions, such as hydrophobic interactions, which leads to fluorescence quenching as shown in **Figure 3.15a** and weak fluorescence brightness compared to formaldehyde as in **Figure 3.15b**.

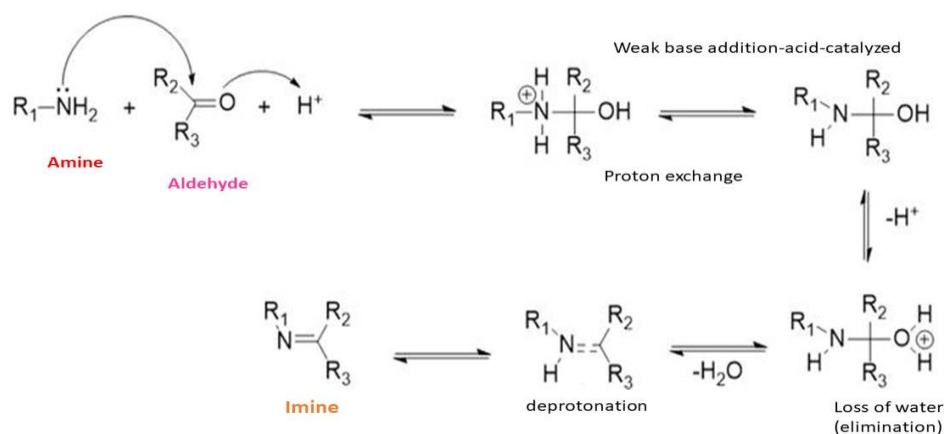


Figure 3.14 The reaction mechanism involved in the formation of imine bond ⁶⁶35.

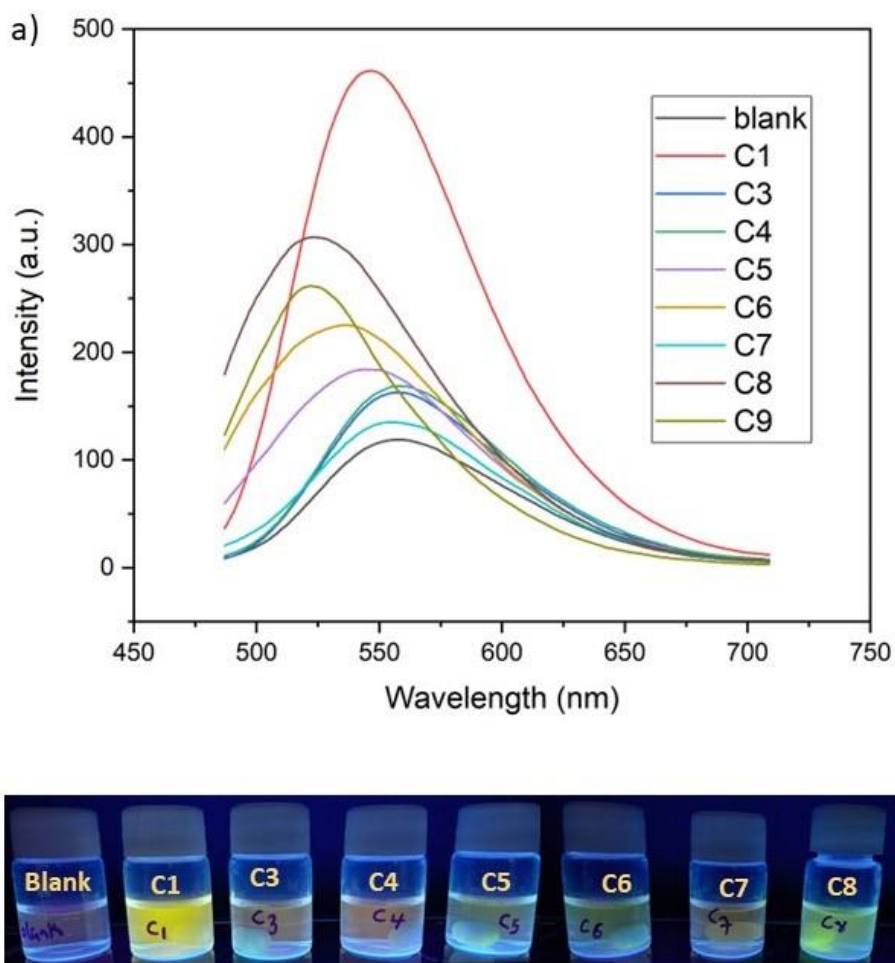


Figure 3.15 Fluorescence spectra of **Naph** (5 μM in acetone) in presence of various aldehydes in 5% DMSO/acetate buffer pH 5.0 ($\lambda_{ex}=455$, slit=5 and PMT= 600) a) and under a 365 nm fluorescence lamp, the addition of different aldehyde species (2 mM in DMSO) resulted in distinct changes in the visual fluorescence of the **Naph** dye. The tested aldehyde species included blank (**Naph**), formaldehyde (C1), propanal (C3), butanal (C4), pentanal (C5), hexanal (C6), heptanal (C7), octanal (C8), and nonanal (C9). These experiments were conducted in a 20 mM acetate buffer with a pH of 5.0 (b)³⁶.

3.9 Optimization of the sensing system for long-chain aldehydes detection

Typically, to produce highly effective biosensors, factors for biological detection in real life must be designed and optimised. Several significant factors, such as reaction time, temperature, pH of the system, and sensor concentration, directly influence the

sensitivity and selectivity of a sensing system. Nevertheless, the vast majority of sensing platforms for biological detection methods are typically used in ambient conditions. Consequently, the temperature factor is irrelevant to our project. In our research, we focused on optimising the sensing conditions such as ratio of EC and **Naph**, pH and reaction time, for identifying long-chain aldehydes.

3.9.1 Study on pH effect of EC@Naph nanosensors for long-chain aldehydes detection

To validate pH effect on sensitivity of fluorescent nanosensor, **EC@Naph** nanosensors were analyzed with nonanal, as long-chain aldehyde, at pH levels of 3.0, 4.0, 5.0, 6.0, 7.0, 7.4, and 8.0 with different buffers. Under a reaction time of 2.0 min, the strong fluorescent signal of the nanosensors was observed at 525 nm. The experiment involved measuring the relative fluorescence intensity of **EC@Naph** nanosensors when react to nonanal. This crucial parameter would provide insights into the ideal pH for the chemical reaction between **EC@Naph** and long-chain aldehydes. As in **Figure 3.16a** and **3.16b**, the result plainly demonstrated that the nanosensors exhibit high fluorescence intensity in descending order at pH 3.0, 4.0, 5.0, 6.0, 7.0, 7.4 and 8.0. Because of our findings, we hypothesized that the interaction between nonanal aldehyde and hydrazine, based on the **Naph** dye, predominantly occurs through imine or Schiff base formation, particularly under acidic conditions. For the acidic solution, pH 3.0 to 6.0, **EC@Naph** nanosensors for nonanal exhibited high fluorescence intensities. Nonetheless, the nanosensors can be applied to study long-chain aldehydes in real samples. Considering the pH of 3.0, which falls under the category of a highly acidic condition, we have concerns regarding its potential detrimental effects on the integrity of living structures in living samples, such as by denaturing their essential structure. The pH 3.0 sensing platform was inappropriate for its intended applications in sensing study. Therefore, after careful evaluation, we have determined that the 20 mM acetate buffer at pH 5.0 is the optimal condition for our sensing system. It exhibits the desirable properties for effective application in real sample sensing, while maintaining a reasonable fluorescent intensity value.

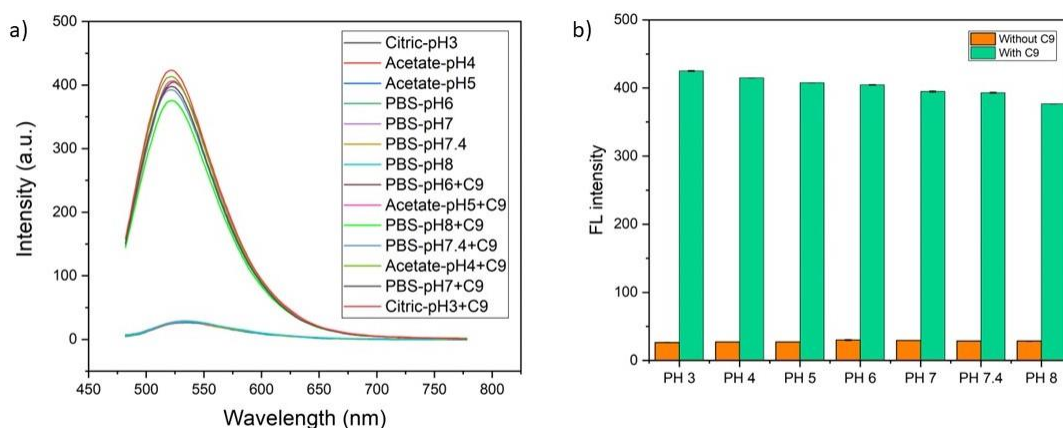


Figure 3.16 Fluorescence intensity of **EC@Naph** nanosensors in the absence and presence of nonanal (2 mM in DMSO). The buffer solutions used were pH 3.0 citric buffer, pH 4.0 and 5.0 acetate buffer, and pH 6.0, 7.0, 7.4, and 8.0 phosphate buffer (PBS). The measurements were made using a wavelength for excitation (λ_{ex}) of 450 nm, PMT 600 V, and a slit of 5 nm a) and Fluorescence spectra of **EC@Naph** nanosensors in the absence and presence of nonanal b)37.

3.10 Selectivity of **EC@Naph** nanosensors

For specific long-chain aldehydes detection, the selectivity of the nanosensor was a crucial characteristic. The ratio between the amount of EC and **Naph** used to form nanoparticles also had a significant part in selecting the best encapsulation of fluorescent dyes for the highly promising selectivity of long-chain aldehydes. In addition to the unique affinity-sensing approach, the development of highly sensitive materials is essential for ensuring effective detection capabilities. For the formation of **EC@Naph** nanoparticles, we then used excess of EC polymer relative to the amount fluorophore **Naph**. Consequently, **EC@Naph** nanosensors were fabricated using various ratios of EC and **Naph**, including 0.5:1.0, 1.0:1.0, 1.5:1.0, and 2.0:1.0 in an attempt to determine the optimal ratio for achieving best fluorescence signals regarding long-chain aldehydes, we investigated **EC@Naph** nanosensors among different variety of organic guests (2 mM) under 2.0 minutes of stirring in a 5% v/v DMSO/acetate buffer at pH 5.0 at ambient temperature. The experimental outcomes were monitored by observing changes in fluorescence. The organic substances

utilized as study guests were frequently present in natural oils.¹⁰⁸⁻¹¹², plasma solutions of human blood^{113, 114}, human urine^{115, 116}, and exhaled breath of lung cancer patients¹¹⁷⁻¹²⁰. They included both the short-chain aldehyde group (formaldehyde, propanal, butanal, and pentanal) and the long-chain aldehyde group (hexanal, heptanal, octanal, and nonanal). **Figures 3.17 to Figure 3.20** depict the sensing efficiencies and selectivity of **EC@Naph** nanosensors with different ratios of EC and **Naph** (0.5:1.0, 1.0:1.0, 1.5:1.0, and 2.0:1.0) concerning various organic compounds. The relative fluorescence signals ($I-I_0$) were significantly enhanced when the long-chain aldehydes, especially octanal and nonanal, were added. These results indicate that **EC@Naph** nanosensors exhibit remarkable selectivity for detecting long-chain aldehydes. Furthermore, we observed that the fluorescence responses increased proportionally with the lengths of aldehyde compounds possessing aliphatic carbon chains. This finding confirms that the hydrophobicity of the long-chain aldehyde family plays a crucial role in the efficient encapsulation of EC, enabling the distinction of long-chain aldehydes derived from several types of aldehydes through hydrophobic-hydrophobic interactions with their alkyl chain length. Additionally, for the detection of short-chain aldehydes, we hypothesized that their hydrophilic properties make it unlikely for them to penetrate the hydrophobic nanoparticles and preferentially undergo induced-fit backbone encapsulation. It suggests that the EC polymers, potentially playing the role of a membrane that is permeable, play a vital role in discriminating between hydrophobic and hydrophilic phases, thereby enhancing the sensitivity of this sensor system.

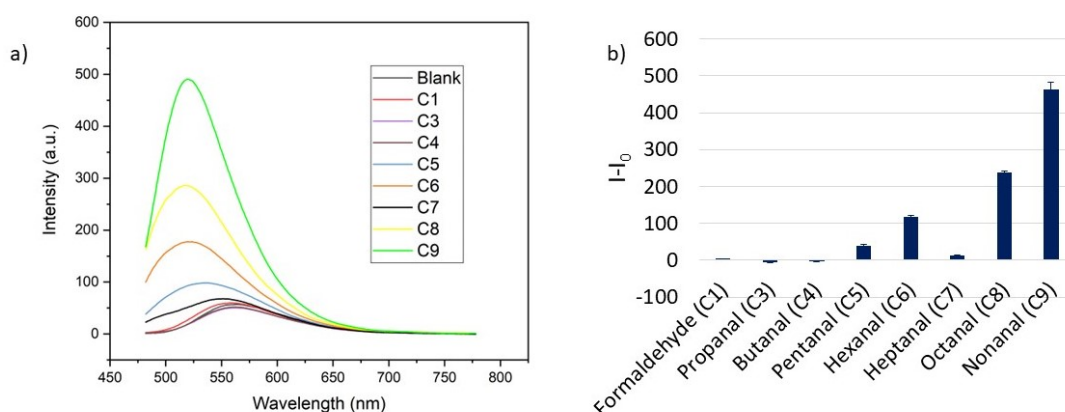


Figure 3.17 (a) Fluorescence spectra and (b) enhancement of relative fluorescence intensity ($I-I_0$) of **EC@Naph** prepared in aqueous solution with a 0.5:1.0 ratio of EC to **Naph**. The measurements were conducted in acetate buffer (20 mM, pH 5.0) in the presence of various aldehyde compounds (2 mM in DMSO). Upon 450nm excitation, 550 V PMT and 5 nm a slit width. The error bar represents the results obtained from at least three measurement values³⁸.

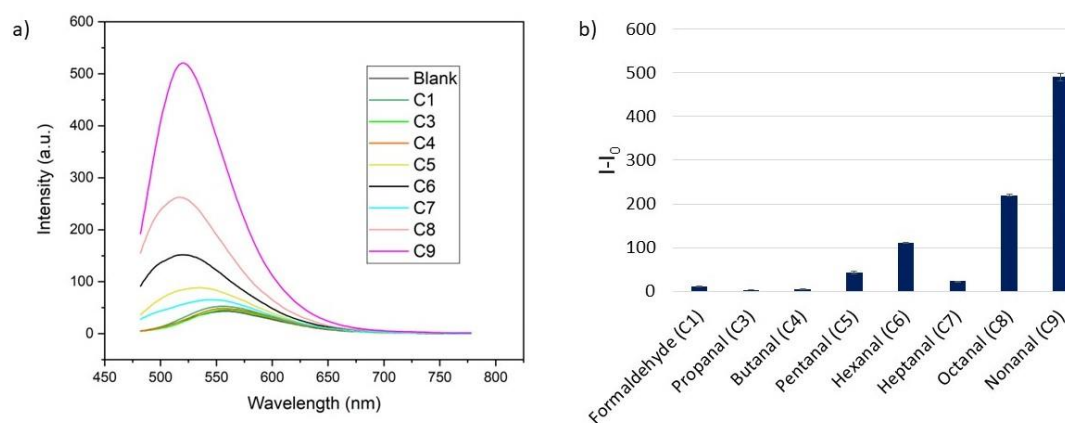


Figure 3.18 (a) Fluorescence spectra and (b) enhancement of relative fluorescence intensity ($I-I_0$) of **EC@Naph** prepared in aqueous solution with a 1.0:1.0 ratio of EC to **Naph**. The measurements were conducted in acetate buffer (20 mM, pH 5.0) in the presence of various aldehyde compounds (2 mM in DMSO). Upon 450nm excitation, 550 V PMT and 5 nm a slit width. The error bar represents the results obtained from at least three measurement values³⁹.

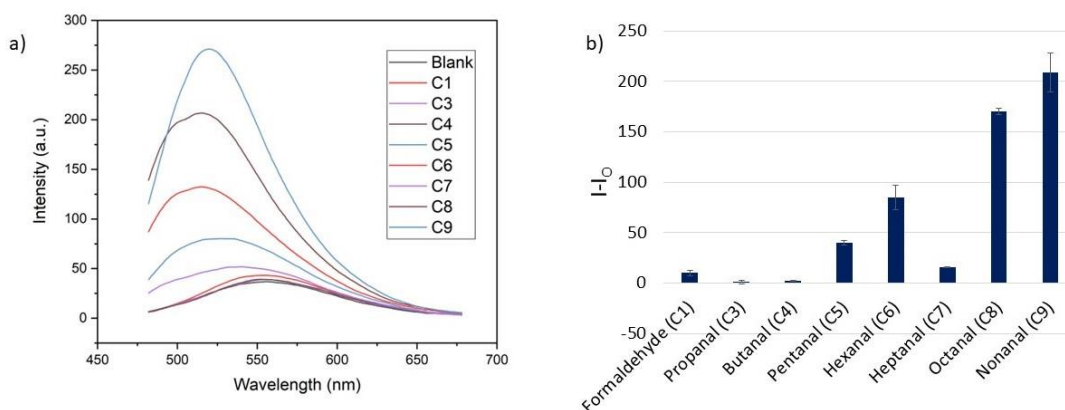


Figure 3.19 (a) Fluorescence spectra and (b) enhancement of relative fluorescence intensity ($I-I_0$) of **EC@Naph** prepared in aqueous solution with a 1.5:1.0 ratio of EC to **Naph**. The measurements were conducted in acetate buffer (20 mM, pH 5.0) in the presence of various aldehyde compounds (2 mM in DMSO). Upon 450nm excitation, 550 V PMT and 5 nm a slit width. The error bar represents the results obtained from at least three measurement values⁴⁰.

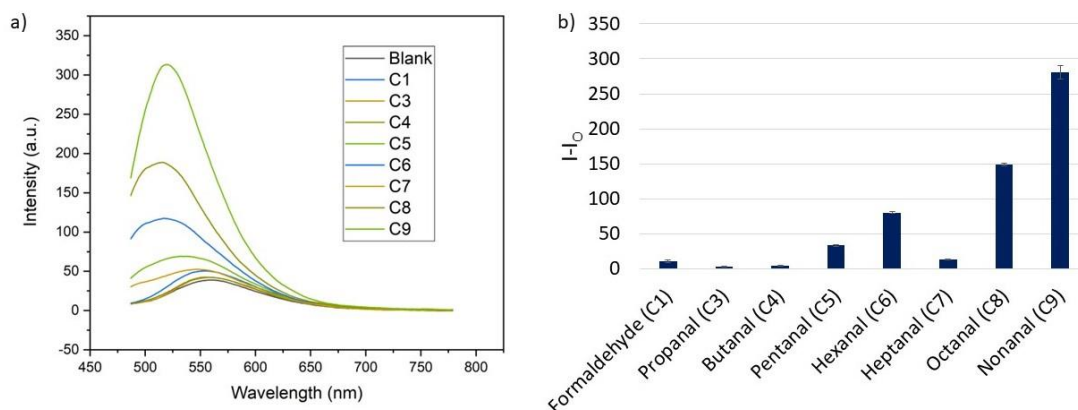


Figure 3.20 (a) Fluorescence spectra and (b) enhancement of relative fluorescence intensity ($I-I_0$) of **EC@Naph** prepared in aqueous solution with a 2.0:1.0 ratio of EC to **Naph**. The measurements were conducted in acetate buffer (20 mM, pH 5.0) in the presence of various aldehyde compounds (2 mM in DMSO). Upon 450nm excitation, 550 V PMT and 5 nm a slit width. The error bar represents the results obtained from at least three measurement values⁴¹.

Based on studies of selectivity, all ratios of EC to **Naph** exhibited the highest fluorescence intensity with nonanal compared to the other guest. Nonetheless, this sensing platform's primary purpose was to detect long-chain aldehydes using a highly efficient method. Thus, the nano sensing platform based on a 1.0:1.0 ratio of EC and **Naph** caused the fluorescent intensity to change significantly during investigation of long-chain aldehyde derivatives, notably octanal and nonanal, this prompted us to choose the 1:1 ratio of EC and **Naph** due to the promising results obtained for the construction of **EC@Naph** nanosensors.

Examining the use of **EC@Naph** nanosensors for the long-chain aldehydes sensing via luminescent visualisation is a topic of recent interest in the field of naked-eye detection. **EC@Naph** nanosensors and 2 mM of aldehyde compounds were vigorously stirred for 2.0 minutes at ambient temperature in a 5% v/v DMSO/acetate buffer with a pH of 5.0. The brightness of **EC@Naph** was monitored upon exposed to a 365 nm UV lamp. As depicted in **Figure 3.21**, the **EC@Naph** nanosensors when various aldehyde guests are present demonstrated dramatic variations in fluorescent brightness at 2 mM concentration. This visual detection is conspicuously according to the fluorescence processes. Considering all the results, we are assured that these sensing materials can serve as a significant improvement in terms of simple, effective, and convenient for detecting particular long-chain aldehyde by naked-eye detection. Long-chain aldehydes with hydrophobic hydrocarbon chains, such as octanal and nonanal, can interact favourably with the hydrophobic portions of the ethyl cellulose matrix. These hydrophobic interactions can aid in the long-chain aldehydes' encapsulation and retention inside the ethyl cellulose matrix, improving their accessibility to naphthalimide and leading to a higher fluorescence brightness, as shown in **Figure 3.21**. Furthermore, short-chain aldehydes including formaldehyde, propanal, and butanal, on the other hand, have weaker hydrophobic interactions, which resulted in less effective encapsulation and reduced selectivity. Additionally, with octanal and nonanal, naphthalimide exhibits higher solubility and greater encapsulation efficiency, producing brighter fluorescence signals. Whereas formaldehyde and other aldehydes might be less soluble in compatible with the ethyl cellulose matrix, resulting in weak fluorescence responses as in **Figure 3.21**.



Figure 3.21 Fluorescence images of **EC@Naph** nanosensors with the addition of different aldehyde species (2 mM in DMSO) including the blank (**EC@Naph**), (C1) formaldehyde, (C3) propanal, (C4) butanal, (C5) pentanal, (C6) hexanal, (C7) heptanal, (C8) octanal, and (C9) nonanal. The measurements were conducted in 20 mM acetate buffer at pH 5.0 under a 365 nm UV irradiation⁴².

3.11 The interaction study between **EC@Naph** with nonanal by fluorescence titration

To examine the sensitivity of our system, we conducted a quantitative analysis of **EC@Naph** nanosensors. Given its highly selective detection, we selected nonanal as the representative long-chain aldehyde for fluorescence titration. This allowed us to determine its concentration and evaluate the system's sensitivity under optimal experimental conditions. The **EC@Naph** and nonanal titration curves were plotted between various concentrations of nonanal, and relative fluorescence intensity ($I-I_0$) before and after the addition of nonanal assigned as I_0 and I , respectively. In this regard, the minimum concentration of quantitative analysis was a crucial factor in determining the sensitivity of the sensory approach. The fluorescence titration curves showed S curve. As expected, a low concentration of nonanal would likely result in the formation of micelle-like nanoparticles that are of poor quality, giving the little fluorescence change at low concentration. However, at high concentrations of nonanal, the fluorescence intensities of nanosensors increased dramatically until unchanged, implying likely the saturation point or complete binding complexes and encapsulation. As shown in **Figure 3.22**, The lengthy alkyl side chain on the aldehyde molecules was what gave this sensation system its sensitivity. This is due to the most influential factor of hydrophobic property of long-chain aldehydes in specific sensing affinity. Considering the aforementioned information, **EC@Naph** prepared with a 1:1

ratio of EC and **Naph** has generated a great deal of interest due to its superior sensing affinity for the detection of long-chain aldehydes. The limit of detection (LOD) together with limit of quantification (LOQ) were computed using equation (1) and (2)¹²¹, the **EC@Naph** nanosensor (1:1) exhibited low LOD and LOQ values of approximately 41 μM and 275 μM , respectively. This indicates that this nanosensor is sensitive to nonanal due to the appropriate lengthy alkyl chain on the aldehyde compounds.

$$LOD = \frac{3SD}{Slope} \quad (1)$$

$$LOQ = \frac{10SD}{Slope} \quad (2)$$

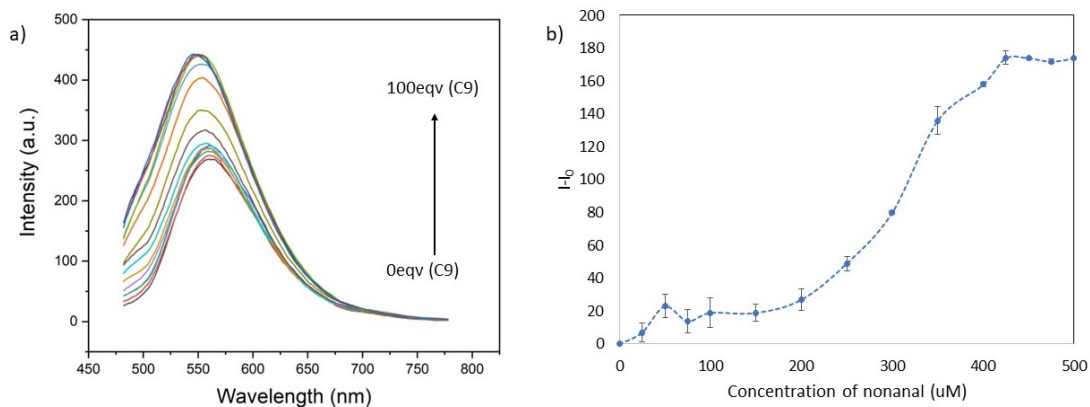


Figure 3.22 (a) Fluorescence spectra and (b) plot illustrating the enhancement of relative fluorescence intensity ($I-I_0$) of **EC@Naph** in an aqueous solution with a 1.0:1.0 ratio of EC to **Naph**. The measurements were performed upon the addition of different nonanal concentrations ranging from 0.0 to 500 μM in acetate buffer (20 mM, pH 5.0)⁴³.

3.12 Quantitative Analysis of EC@Naph for Nonanal Detection Using Naked-Eye Observation

In our ongoing search we devised a method for determining the concentration of long-chain aldehyde based on visual observation to enable quantitative evaluation of the sensing system using naked-eye detection. In the experiment, **EC@Naph** nanosensors were employed, and nonanal concentrations ranging from 0.00 to 1.50 mM were tested in a 5% DMSO/acetate buffer with a pH of 5.0. As depicted in **Figure 3.23**, UV irradiation at 365 nm was used to observe variations in the sensor platform's fluorescence brightness. upon binding with nonanal. The lowest detectable concentration of nonanal by micellar **EC@Naph** nanosensors using naked-eye detection was found to be 50 μM according to the observable changes from darkness to initially yellow brightness. This additional sensing platform may produce the most interesting characteristic of lung cancer pre-screening diagnosis, in accordance with expectations.



Figure 3.23 Fluorescence images of **EC@Naph** nanosensors (3.5% v/v) obtained by adding different concentrations of nonanal (in DMSO): blank (**EC@Naph**), (I) 1 μM , (II) 5 μM , (III) 10 μM , (IV) 50 μM , (V) 100 μM , (VI) 1.0 mM, and (VII) 1.5 mM.

The measurements were conducted in 20 mM acetate buffer at pH 5.0 under a 365 nm UV lamp⁴⁴.

3.13 Interference study

Considering the crucial role of diagnostic purposes using sensing methods, the interference caused by organic compounds emerged as a significant concern for the sensing platform. However, before delving into the sensing efficiency of the sensing platform in real samples, it was crucial to address the potential interferences posed by organic compounds with similar electronic structures to aldehyde compounds. In the

context of nonanal sensing, we investigated the fluorescence responses at 551 nm of **EC@Naph** in the presence of various aldehyde derivatives, such as formaldehyde (FA), propanal (PRO), and benzaldehyde (BA). Additionally, we examined the impact of major components found in plasma and exhaled breath of lung cancer, that include glucose (GLU), sucrose (SUC), lysine (LYS), phenylalanine (PHE), glutathione (GLUTA), urea, and NaCl salts, these compounds were selected as potential candidates. The results presented in **Figure 3.24** demonstrate that the introduction of biological interferent compounds into a mixture of **EC@Naph** and nonanal in a 5% v/v DMSO/acetate buffer at pH 5.0 at ambient temperature did not cause significant alteration in the fluorescence emissions at 551 nm (blue bar) with respect to the free nonanal emission (orange bar). The results demonstrated that the fluorescence signals of **EC@Naph** for nonanal detection were not significantly affected by the mixture of simulated blood samples and exhaled breath components present in lung cancer patients. This observation further confirms the importance of the hydrophobic interaction between long-alkyl chain aldehydes and **EC@Naph**, as well as the reaction between hydrazine and the aldehyde group. These mechanisms play a vital role in the changes observed in fluorescence responds.

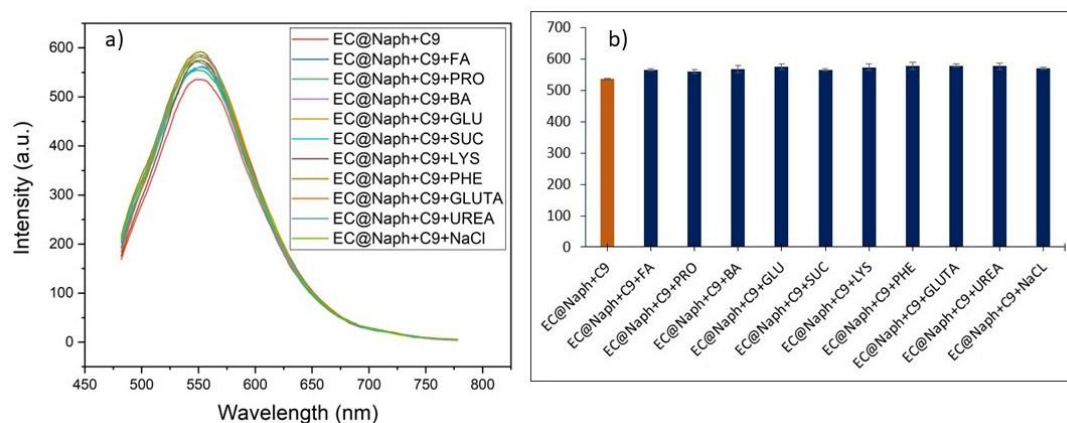
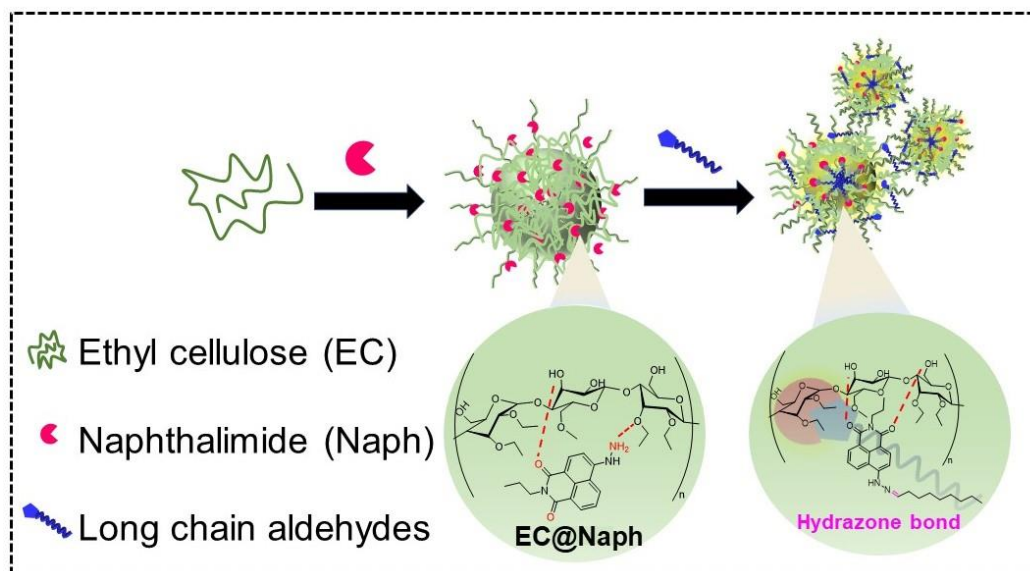


Figure 3.24 (a) Fluorescence intensity and (b) plot illustrating the relative fluorescence responses of **EC@Naph** upon the addition of nonanal (500 μM in DMSO) alongside short-chain aldehyde species and major plasma and lung fluid compounds (500 μM in DMSO) in acetate buffer (20 mM, pH 5.0). The findings were made using λ_{em} of 450 nm, a PMT of 650 V, and a slit of 10 nm⁴⁵.

CHAPTER IV CONCLUSION

4.1 Conclusion

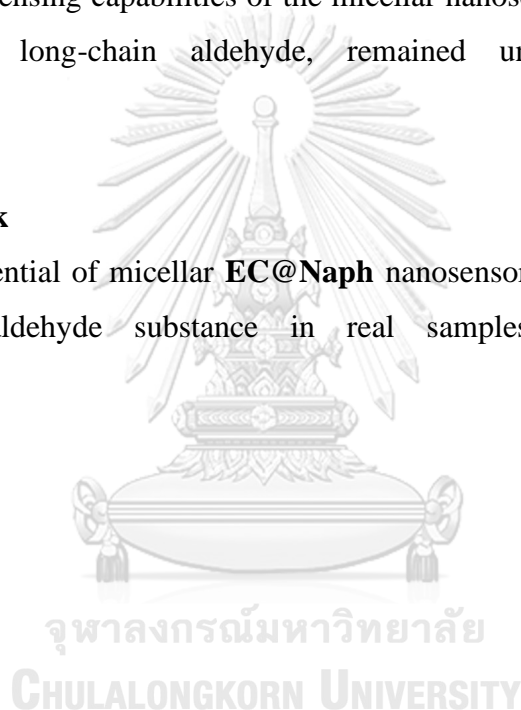


In conclusion, we have created and analyzed water-soluble fluorescence nanosensors through encapsulating naphthalimide dyes in the ethyl cellulose backbone by varying the ratio of EC and **Naph** dye components for the development of an efficient nanosensor capable of detecting long-chain aldehydes in aqueous media. Various ratios of EC and **Naph** were used that include 0.5:1.0, 1.0:1.0, 1.5:1.0, and 2.0:1.0, respectively. The 1.0:1.0 was used as the optimized ratio for sensing application. The sensitivity and selectivity of the **EC@Naph** nanosensors for detecting long-chain aldehydes have been successfully developed in aqueous solutions. This sensing system aligns with our concept, which involves the utilization of incomplete micellar nanoparticles prior to the binding with long-chain aldehyde compounds. When introduced, the long-chain aldehydes preferentially penetrate the core of the micellar nanoparticles as a result of hydrophobic nature of the system, acting as the driving force. Subsequently, they undergo covalent reactions with hydrazine-functionalized dyes through hydrazone formation. This unique mechanism enables the distinction of long-chain aldehydes from other compounds. Interestingly, self-assembly encapsulation hydrophobic-hydrophobic interaction induced the highly complete encapsulation by promoting robust fluorescence enhancement. Additionally, the

fluorescence responses of **EC@Naph** nanosensors exhibited a proportional increase corresponding to the concentration of long-chain aldehydes, particularly nonanal, at pH 5.0, with a quick response time of 2 minutes at ambient temperature. This sensing system demonstrated high selectivity for long-chain aldehydes, specifically nonanal, boasting a low detection limit. Notably, the nanosensor displayed remarkable selectivity towards nonanal, with a limit of detection (LOD) of 41 μM and a limit of quantification (LOQ) of 275 μM . The developed nanosensor holds significant potential for the sensitive detection of long-chain aldehydes in aqueous media. Furthermore, the sensing capabilities of the micellar nanosensors towards nonanal, as a representative long-chain aldehyde, remained unaffected by significant interferences.

4.2 Future work

The detecting potential of micellar **EC@Naph** nanosensors for detection of nonanal as long-chain aldehyde substance in real samples will be investigated.



REFERENCES

1. Wilson, A. J.; , Supramolecular chemistry, *Annu. Rep. Prog. Chem.* **104**, 164-183.
2. Biedermann, F.; ; Schneider, H. J.; , Experimental binding energies in supramolecular complexes. *Chem. Rev.* **116**, 5216-5300.
3. Fischer, E.; , Influence of configuration on the action of enzymes. *Acc. Chem. Res.* **3**, 2985-2993.
4. Desiraju, G. R.; , The all-chemist Linus Pauling set the agenda for a century of chemical research. *Chem. Rev.* **408**.
5. Lehn, J. M.; , From supramolecular chemistry towards constitutional dynamic chemistry and adaptive chemistry. *Chem. Rev.* **36**, 151-160.
6. Oshovsky, G. V.; ; Reinhoudt, D. N.; ; Verboom, W.; , Supramolecular chemistry in water, *Angew Chem.* **46**, 2366-2393.
7. Lehn, J. M.; , Towards complex matter: supramolecular chemistry and self-organization. *Chem. Rev.* **17**, 263-280.
8. Eigen, M.; , Selforganization of matter and the evolution of biological macromolecules. *Chem. Rev.* **58**, 465-523.
9. Lehn, J.-M.; , Perspectives in Supramolecular Chemistry—From Molecular Recognition towards Molecular Information Processing and Self-Organization. *Chem. Rev.* **29**, 1304-1319.
10. Balzani, V.; ; Gómez-López, M.; ; Stoddart, J. F.; , Molecular Machines. *Chem. Rev.* **31**, 405-414.
11. Ikeda, T.; ; Stoddart, J. F.; , Electrochromic materials using mechanically interlocked molecules. *Chem. Rev.* **9**, 14104.
12. Zhang, S.; , Fabrication of novel biomaterials through molecular self-assembly. *Chem. Rev.* **21**, 1171.
13. Dickert, L.; ; F.; ; Hayden, O.; , Molecular imprinting in chemical sensing. *Chem. Rev.* **18**.
14. Siraj, N.; El-Zahab, B.; Hamdan, S.; Karam, T. E.; Haber, L. H.; Li, M.; Fakayode, S. O.; Das, S.; Valle, B.; Strongin, R. M., Fluorescence, phosphorescence, and chemiluminescence. *Analytical chemistry* **2016**, *88* (1), 170-202.
15. Rabinowitch, E., Fluorescence and phosphorescence. ACS Publications: 1951.
16. McGlynn, S., Fluorescence and Phosphorescence Analysis. Principles and Applications. *Journal of the American Chemical Society* **1966**, *88* (23), 5688-5688.

17. Dave, B. S. *Metal Complex Interactions with Metal-Modified Nucleic Acids*. University of Zurich, 2016.
18. <https://www.simtrum.com/WebShop/SolutionInfo.aspx?id=1669> (accessed 15/05/2023).
19. Park, S.-H.; Kwon, N.; Lee, J.-H.; Yoon, J.; Shin, I., Synthetic ratiometric fluorescent probes for detection of ions. *Chemical Society Reviews* **2020**, *49* (1), 143-179.
20. Li, X.; Qu, H.; Wang, Y.; Zhang, X.; Bai, L.; Wang, Z., Fluorescent probe for detection of formaldehyde based on UiO-66-NH₂. *Journal of Solid State Chemistry* **2023**, *317*, 123672.
21. Hu, Y.; Guo, S.; Peng, J.; Fan, Y.; Wang, F.; Lu, L.; Fu, H.; Chen, X.; She, Y., Ratiometric Pyrene-Based Fluorescent Sensor for On-site Monitoring of Formaldehyde in Foods and Living Cells. *Sensors and Actuators B: Chemical* **2023**, 134064.
22. Wang, L.; Wang, J.; Xu, J.; Liu, S.; Huang, S.; Han, S.; Liu, Y.; Lv, M., Highly sensitive qualitative and quantitative detection of saturated fatty aldehydes in edible vegetable oils using a “turn-on” fluorescent probe by high performance liquid chromatography. *Journal of Chromatography A* **2020**, *1621*, 461063.
23. Martínez-Aquino, C.; Costero, A. M.; Gil, S.; Gaviña, P., Resorcinol functionalized gold nanoparticles for formaldehyde colorimetric detection. *Nanomaterials* **2019**, *9* (2), 302.
24. March, J.; Brown, W. H. Aldehyde. <https://www.britannica.com/science/aldehyde> (accessed 20/05/2023).
25. Wang, M.; Li, Q.; Li, E.; Liu, J.; Zhou, J.; Huang, F., Vapochromic Behaviors of A Solid-State Supramolecular Polymer Based on Exo-Wall Complexation of Perethylated Pillar [5] arene with 1, 2, 4, 5-Tetracyanobenzene. *Angewandte Chemie* **2021**, *133* (15), 8196-8201.
26. Hirao, T.; Fukuta, K.; Haino, T., Supramolecular approach to polymer-shape transformation via calixarene–fullerene complexation. *Macromolecules* **2020**, *53* (9), 3563-3570.
27. Chen, S.; Jia, Y.; Zou, G.-Y.; Yu, Y.-L.; Wang, J.-H., A ratiometric

fluorescent nanoprobe based on naphthalimide derivative-functionalized carbon dots for imaging lysosomal formaldehyde in HeLa cells. *Nanoscale* **2019**, *11* (13), 6377-6383.

28. Xia, L.; Du, Y.; Xiao, X.; Li, G., One-step membrane protected micro-solid-phase extraction and derivatization coupling to high-performance liquid chromatography for selective determination of aliphatic aldehydes in cosmetics and food. *Talanta* **2019**, *202*, 580-590.
29. Liu, Y.; Shangguan, L.; Shi, B., A multi-responsive cross-linked supramolecular polymer network constructed by mussel yield coordination interaction and pillar [5] arene-based host-guest complexation. *Chemical Communications* **2018**, *54* (86), 12230-12233.
30. Zhang, J.; Qiu, H.; He, T.; Li, Y.; Yin, S., Fluorescent supramolecular polymers formed by crown ether-based host-guest interaction. *Frontiers in Chemistry* **2020**, *8*, 560.
31. Li, E.; Jie, K.; Zhou, Y.; Zhao, R.; Zhang, B.; Wang, Q.; Liu, J.; Huang, F., Aliphatic aldehyde detection and adsorption by nonporous adaptive pillar [4] arene [1] quinone crystals with vapochromic behavior. *ACS applied materials & interfaces* **2018**, *10* (27), 23147-23153.
32. Konar, S.; Samanta, D.; Mandal, S.; Das, S.; Mahto, M. K.; Shaw, M.; Mandal, M.; Pathak, A., Selective and sensitive detection of cinnamaldehyde by nitrogen and sulphur co-doped carbon dots: a detailed systematic study. *RSC advances* **2018**, *8* (74), 42361-42373.
33. Zhu, H.; She, J.; Zhou, M.; Fan, X., Rapid and sensitive detection of formaldehyde using portable 2-dimensional gas chromatography equipped with photoionization detectors. *Sensors and Actuators B: Chemical* **2019**, *283*, 182-187.
34. Liu, Y.; Lou, B.; Shangguan, L.; Cai, J.; Zhu, H.; Shi, B., Pillar [5] arene-based organometallic cross-linked polymer: synthesis, structure characterization, and catalytic activity in the Suzuki-Miyaura coupling reaction. *Macromolecules* **2018**, *51* (4), 1351-1356.
35. Ruengsuk, A.; Khamphaijun, K.; Pananusorn, P.; Docker, A.; Tantirungrotechai, J.; Sukwattanasinitt, M.; Harding, D. J.; Bunchuay, T., Pertosylated pillar [5] arene: self-template assisted synthesis and supramolecular polymer formation.

Chemical Communications **2020**, 56 (62), 8739-8742.

36. Yang, H.-L.; Li, Z.-H.; Liu, P.-P.; Sun, X.-W.; Wang, Z.-H.; Yao, H.; Zhang, Y.-M.; Wei, T.-B.; Lin, Q., Metal-free white light-emitting fluorescent material based on simple pillar [5] arene-tripodal amide system and theoretical insights on its assembly and fluorescent properties. *Langmuir* **2020**, 36 (45), 13469-13476.
37. Hesslow, G.; Svensson, P.; Ivarsson, M., Learned movements elicited by direct stimulation of cerebellar mossy fiber afferents. *Neuron* **1999**, 24 (1), 179-185.
38. Ma, C.; Ji, J.; Tan, C.; Chen, D.; Luo, F.; Wang, Y.; Chen, X., Headspace solid-phase microextraction coupled to gas chromatography for the analysis of aldehydes in edible oils. *Talanta* **2014**, 120, 94-99.
39. Luo, X.; Yazdanpanah, M.; Bhooi, N.; Lehotay, D., Determination of aldehydes and other lipid peroxidation products in biological samples by gas chromatography-mass spectrometry. *Analytical Biochemistry* **1995**, 228 (2), 294-298.
40. Yuniati, W.; Amelia, T.; Ibrahim, S.; Damayanti, S., Analytical Method Development for Determining Formaldehyde in Cream Cosmetics Using Hyphenated Gas Chromatography. *ACS omega* **2021**, 6 (42), 28403-28409.
41. Chen, L.; Cai, Y.; Feng, W.; Yuan, L., Pillararenes as macrocyclic hosts: a rising star in metal ion separation. *Chemical Communications* **2019**, 55 (55), 7883-7898.
42. Hao, Q.; Kang, Y.; Xu, J.-F.; Zhang, X., pH/ROS Dual-Responsive Supramolecular Vesicles Fabricated by Carboxylated Pillar [6] arene-Based Host-Guest Recognition and Phenylboronic Acid Pinacol Ester Derivative. *Langmuir* **2020**, 36 (15), 4080-4087.
43. Li, Z.-Y.; Zhang, Y.; Zhang, C.-W.; Chen, L.-J.; Wang, C.; Tan, H.; Yu, Y.; Li, X.; Yang, H.-B., Cross-linked supramolecular polymer gels constructed from discrete multi-pillar [5] arene metallacycles and their multiple stimuli-responsive behavior. *Journal of the American Chemical Society* **2014**, 136 (24), 8577-8589.
44. Zhang, J.; Liu, X.; Wang, J.; Wu, J.; Wang, C.; Qi, H.; Liang, H., Rapid and sensitive detection of formaldehyde based on AC electrokinetic effects. *Micro & Nano Letters* **2018**, 13 (1), 63-68.
45. Liu, X.; Fu, C.; Ren, X.; Liu, H.; Li, L.; Meng, X., Fluorescence switching method for cascade detection of salicylaldehyde and zinc (II) ion using protein protected

gold nanoclusters. *Biosensors and Bioelectronics* **2015**, *74*, 322-328.

46. Wahed, P.; Razzaq, M. A.; Dharmapuri, S.; Corrales, M., Determination of formaldehyde in food and feed by an in-house validated HPLC method. *Food chemistry* **2016**, *202*, 476-483.

47. Swarin, S. J.; Lipari, F., Determination of formaldehyde and other aldehydes by high performance liquid chromatography with fluorescence detection. *Journal of Liquid Chromatography* **1983**, *6* (3), 425-444.

48. Houlgate, P. R.; Dhingra, K. S.; Nash, S. J.; Evans, W. H., Determination of formaldehyde and acetaldehyde in mainstream cigarette smoke by high-performance liquid chromatography. *Analyst* **1989**, *114* (3), 355-360.

49. Possanzini, M.; Di Palo, V., Determination of formaldehyde and acetaldehyde in air by HPLC with fluorescence detection. *Chromatographia* **1997**, *46*, 235-240.

50. Gryllaki-Berger, M.; Mugny, C.; Perrenoud, D.; Pannather, A.; Frenk, E., A comparative study of formaldehyde detection using chromotropic acid, acetylacetone and HPLC in cosmetics and household cleaning products. *Contact Dermatitis* **1992**, *26* (3), 149-154.

51. de Lima, L. F.; Brandão, P. F.; Donegatti, T. A.; Ramos, R. M.; Gonçalves, L. M.; Cardoso, A. A.; Pereira, E. A.; Rodrigues, J. A., 4-hydrazinobenzoic acid as a derivatizing agent for aldehyde analysis by HPLC-UV and CE-DAD. *Talanta* **2018**, *187*, 113-119.

52. Lu, X.; Li, R.; Han, B.; Ma, H.; Hou, X.; Kang, Y.; Zhang, Y.; Wang, J.-J., Fluorescence sensing of formaldehyde and acetaldehyde based on responsive inverse opal photonic crystals: a multiple-application detection platform. *ACS Applied Materials & Interfaces* **2021**, *13* (11), 13792-13801.

53. Dator, R. P.; Solivio, M. J.; Villalta, P. W.; Balbo, S., Bioanalytical and mass spectrometric methods for aldehyde profiling in biological fluids. *Toxics* **2019**, *7* (2), 32.

54. Ge, K.; Yi, L.; Wu, Q.; Li, Y.; Zhang, H.; Gu, Y., Detection of formaldehyde by Surface-Enhanced Raman spectroscopy based on PbBiO₂Br/Au₄Ag₄ nanospheres. *ACS Applied Nano Materials* **2021**, *4* (10), 10218-10227.

55. Zhang, H.; Wu, Z.; Zhi, Z.; Gao, W.; Sun, W.; Hua, Z.; Wu, Y., Practical and Efficient: A Pocket-Sized Device Enabling Detection of Formaldehyde Adulteration in

Vegetables. *ACS omega* **2021**, 7 (1), 160-167.

56. Promsuwan, K.; Saichanapan, J.; Soleh, A.; Saisahas, K.; Kanatharana, P.; Thavarungkul, P.; Tayayuth, K.; Guo, C. X.; Li, C. M.; Limbut, W., Portable flow injection amperometric sensor consisting of Pd nanochains, graphene nanoflakes, and WS₂ nanosheets for formaldehyde detection. *ACS Applied Nano Materials* **2021**, 4 (11), 12429-12441.

57. Kazemifard, A. G.; Moore, D. E.; Mohammadi, A., Polarographic determination of benzaldehyde in benzyl alcohol and sodium diclofenac injection formulations. *Journal of pharmaceutical and biomedical analysis* **2002**, 30 (2), 257-262.

58. Moreno López, L. J.; Callejón Mochón, M.; Jiménez Sánchez, J. C.; Bello López, M. A.; Guiraúm Pérez, A., Electrochemical reduction of benzaldehyde as its Girard-P derivative at the mercury electrode and differential-pulse polarographic determination of benzaldehyde. *Microchimica Acta* **2001**, 137, 19-24.

59. Trivedi, D.; Crosse, J.; Tanti, J.; Cass, A. J.; Toghill, K. E., The electrochemical determination of formaldehyde in aqueous media using nickel modified electrodes. *Sensors and Actuators B: Chemical* **2018**, 270, 298-303.

60. Padmalaya, G.; Vardhan, K. H.; Kumar, P. S.; Ali, M. A.; Chen, T.-W., A disposable modified screen-printed electrode using egg white/ZnO rice structured composite as practical tool electrochemical sensor for formaldehyde detection and its comparative electrochemical study with Chitosan/ZnO nanocomposite. *Chemosphere* **2022**, 288, 132560.

61. Nie, X.; Dong, K.; Tian, Y.; Zong, C.; Chen, Z.; Wang, X.; Zhao, Y., A green analysis detection of formaldehyde in grooming products by surface enhanced Raman spectroscopy. *Materials Today Sustainability* **2023**, 22, 100303.

62. Luong, J.; Yang, X.; Hua, Y.; Yang, P.; Gras, R., Gas chromatography with in situ catalytic hydrogenolysis and flame ionization detection for the direct measurement of formaldehyde and acetaldehyde in challenging matrices. *Analytical chemistry* **2018**, 90 (23), 13855-13859.

63. Chen, D.; Ding, J.; Wu, M.-K.; Zhang, T.-Y.; Qi, C.-B.; Feng, Y.-Q., A liquid chromatography–mass spectrometry method based on post column derivatization for automated analysis of urinary hexanal and heptanal. *Journal of Chromatography a*

2017, *1493*, 57-63.

64. Tang, Y.; Ma, Y.; Yin, J.; Lin, W., Strategies for designing organic fluorescent probes for biological imaging of reactive carbonyl species. *Chemical Society Reviews* **2019**, *48* (15), 4036-4048.
65. McCormack, M. P.; Shalumova, T.; Tanski, J. M.; Waters, S. P., Development of a 2-Aza-Cope-[3+ 2] dipolar cycloaddition strategy for the synthesis of quaternary proline scaffolds. *Organic letters* **2010**, *12* (17), 3906-3909.
66. Azab, M. E.; Rizk, S. A.; Amr, A. E.-G. E., Synthesis of some novel heterocyclic and schiff base derivatives as antimicrobial agents. *Molecules* **2015**, *20* (10), 18201-18218.
67. Li, P.; Zhang, D.; Zhang, Y.; Lu, W.; Wang, W.; Chen, T., Ultrafast and efficient detection of formaldehyde in aqueous solutions using chitosan-based fluorescent polymers. *ACS sensors* **2018**, *3* (11), 2394-2401.
68. Lin, M.; Liu, S., Naphthalimide-Based Fluorescent Probe for Profiling of Aldehydes during Oxidation of Unsaturated Lipids. *Journal of Agricultural and Food Chemistry* **2022**, *70* (44), 14304-14311.
69. Li, J.; Hou, C.; Huo, D.; Yang, M.; Fa, H.-b.; Yang, P., Development of a colorimetric sensor Array for the discrimination of aldehydes. *Sensors and Actuators B: Chemical* **2014**, *196*, 10-17.
70. Lin, Q.; Fan, Y.-Q.; Gong, G.-F.; Mao, P.-P.; Wang, J.; Guan, X.-W.; Liu, J.; Zhang, Y.-M.; Yao, H.; Wei, T.-B., Ultrasensitive detection of formaldehyde in gas and solutions by a catalyst replaced sensor based on a pillar [5] arene derivative. *ACS Sustainable Chemistry & Engineering* **2018**, *6* (7), 8775-8781.
71. Goesmann, H.; Feldmann, C., Nanoparticulate functional materials. *Angewandte Chemie International Edition* **2010**, *49* (8), 1362-1395.
72. Li, N.; Liu, D.; Cui, H., Metal-nanoparticle-involved chemiluminescence and its applications in bioassays. *Analytical and bioanalytical chemistry* **2014**, *406*, 5561-5571.
73. Gleiter, H., Nanostructured materials: basic concepts and microstructure. *Acta materialia* **2000**, *48* (1), 1-29.
74. Aversa, R.; Modarres, M. H.; Cozzini, S.; Ciancio, R.; Chiusole, A., The first annotated set of scanning electron microscopy images for nanoscience. *Scientific data*

2018, 5 (1), 1-10.

75. Pokropivny, V.; Skorokhod, V., Classification of nanostructures by dimensionality and concept of surface forms engineering in nanomaterial science. *Materials Science and Engineering: C* **2007**, 27 (5-8), 990-993.
76. Shiau, B.-W.; Lin, C.-H.; Liao, Y.-Y.; Lee, Y.-R.; Liu, S.-H.; Ding, W.-C.; Lee, J.-R., The characteristics and mechanisms of Au nanoparticles processed by functional centrifugal procedures. *Journal of Physics and Chemistry of Solids* **2018**, 116, 161-167.
77. Asghari, F.; Jahanshiri, Z.; Imani, M.; Shams-Ghahfarokhi, M.; Razzaghi-Abyaneh, M., Antifungal nanomaterials: synthesis, properties, and applications. In *Nanobiomaterials in antimicrobial therapy*, Elsevier: 2016; pp 343-383.
78. Saleh, T. A., Nanomaterials: Classification, properties, and environmental toxicities. *Environmental Technology & Innovation* **2020**, 20, 101067.
79. Li, J.; Wang, Y.; Zhang, Q.; Huo, D.; Hou, C.; Zhou, J.; Luo, H.; Yang, M., New application of old methods: Development of colorimetric sensor array based on Tollen's reagent for the discrimination of aldehydes based on Tollen's reagent. *Analytica Chimica Acta* **2020**, 1096, 138-147.
80. Yang, L.; Han, Q.; Ling, X.; Wang, Y.; Li, M.; Chen, Q.; Wang, X., N-Butyl-4-hydrazino-1, 8-naphthalimide-Loaded Chitosan Self-Assembled Nanoparticles as Fluorescent Ratiometric Chemosensors for Detection of Formaldehyde. *ACS Applied Nano Materials* **2022**, 5 (5), 7392-7401.
81. Kumar, M.; Mohajir, A. E.; Berger, F.; Raschetti, M.; Sanchez, J.-B., Dealuminated Zeolite Y/SnO₂ Nanoparticle Hybrid Sensors for Detecting Trace Levels of Propanol as a Lung Cancer Biomarker. *ACS Applied Nano Materials* **2022**, 5 (7), 9170-9178.
82. Torre, L. A.; Siegel, R. L.; Jemal, A., Lung cancer statistics. *Lung cancer and personalized medicine: current knowledge and therapies* **2016**, 1-19.
83. Saalberg, Y.; Bruhns, H.; Wolff, M., Photoacoustic spectroscopy for the determination of lung cancer biomarkers—A preliminary investigation. *Sensors* **2017**, 17 (1), 210.
84. Toyokuni, S.; Okamoto, K.; Yodoi, J.; Hiai, H., Persistent oxidative stress in

cancer. *FEBS letters* **1995**, 358 (1), 1-3.

85. Jongkhumkrong, J.; Thaveesangsakulthai, I.; Sukbangnop, W.; Kulsing, C.; Sooksimuang, T.; Aonbangkhen, C.; Sahasithiwat, S.; Sriprasart, T.; Palaga, T.; Chantaravisoot, N., Helicene-Hydrazide Encapsulated Ethyl Cellulose as a Potential Fluorescence Sensor for Highly Specific Detection of Nonanal in Aqueous Solutions and a Proof-of-Concept Clinical Study in Lung Fluid. *ACS Applied Materials & Interfaces* **2022**, 14 (44), 49495-49507.
86. Staneva, D.; Manov, H.; Yordanova, S.; Vasileva-Tonkova, E.; Stoyanov, S.; Grabchev, I., Synthesis, spectral properties and antimicrobial activity of a new cationic water-soluble pH-dependent poly (propylene imine) dendrimer modified with 1, 8-naphthalimides. *Luminescence* **2020**, 35 (6), 947-954.
87. Sali, S.; Grabchev, I.; Chovelon, J.-M.; Ivanova, G., Selective sensors for Zn²⁺ cations based on new green fluorescent poly (amidoamine) dendrimers peripherally modified with 1, 8-naphthalimides. *Spectrochimica Acta Part A: Molecular and Biomolecular Spectroscopy* **2006**, 65 (3-4), 591-597.
88. Said, A. I.; Georgiev, N. I.; Bojinov, V. B., A novel dual naked eye colorimetric and fluorescent pH chemosensor and its ability to execute three INHIBIT based digital comparator. *Dyes and Pigments* **2022**, 205, 110489.
89. Zhang, S.; Wang, Y.; Xu, H., A new naphthalimide-picolinohydrazide derived fluorescent “turn-on” probe for hypersensitive detection of Al³⁺ ions and applications of real water analysis and bio-imaging. *Spectrochimica Acta Part A: Molecular and Biomolecular Spectroscopy* **2022**, 275, 121193.
90. Said, A. I.; Georgiev, N. I.; Bojinov, V. B., A fluorescent bichromophoric “off-on-off” pH probe as a molecular logic device (half-subtractor and digital comparator) operating by controlled PET and ICT processes. *Dyes and Pigments* **2019**, 162, 377-384.
91. Grabchev, I.; Dumas, S.; Chovelon, J.-M.; Nedelcheva, A., First generation poly (propyleneimine) dendrimers functionalised with 1, 8-naphthalimide units as fluorescence sensors for metal cations and protons. *Tetrahedron* **2008**, 64 (9), 2113-2119.
92. Staneva, D.; Said, A. I.; Vasileva-Tonkova, E.; Grabchev, I., Enhanced

photodynamic efficacy using 1, 8-naphthalimides: Potential application in antibacterial photodynamic therapy. *Molecules* **2022**, *27* (18), 5743.

93. Duke, R. M.; Veale, E. B.; Pfeffer, F. M.; Kruger, P. E.; Gunnlaugsson, T., Colorimetric and fluorescent anion sensors: an overview of recent developments in the use of 1, 8-naphthalimide-based chemosensors. *Chemical society reviews* **2010**, *39* (10), 3936-3953.

94. Meher, N.; Panda, S.; Kumar, S.; Iyer, P. K., Aldehyde group driven aggregation-induced enhanced emission in naphthalimides and its application for ultradetection of hydrazine on multiple platforms. *Chemical science* **2018**, *9* (16), 3978-3985.

95. Geraghty, C.; Wynne, C.; Elmes, R. B., 1, 8-Naphthalimide based fluorescent sensors for enzymes. *Coordination Chemistry Reviews* **2021**, *437*, 213713.

96. Banerjee, S.; Veale, E. B.; Phelan, C. M.; Murphy, S. A.; Tocci, G. M.; Gillespie, L. J.; Frimannsson, D. O.; Kelly, J. M.; Gunnlaugsson, T., Recent advances in the development of 1, 8-naphthalimide based DNA targeting binders, anticancer and fluorescent cellular imaging agents. *Chemical Society Reviews* **2013**, *42* (4), 1601-1618.

97. Hakim, M.; Broza, Y. Y.; Barash, O.; Peled, N.; Phillips, M.; Amann, A.; Haick, H., Volatile organic compounds of lung cancer and possible biochemical pathways. *Chemical reviews* **2012**, *112* (11), 5949-5966.

98. Guadagni, R.; Miraglia, N.; Simonelli, A.; Silvestre, A.; Lamberti, M.; Feola, D.; Acampora, A.; Sannolo, N., Solid-phase microextraction–gas chromatography–mass spectrometry method validation for the determination of endogenous substances: urinary hexanal and heptanal as lung tumor biomarkers. *Analytica Chimica Acta* **2011**, *701* (1), 29-36.

99. Xu, H.; Wang, S., A novel sorptive extraction method based on polydimethylsiloxane frit for determination of lung cancer biomarkers in human serum. *Analytica chimica acta* **2012**, *724*, 61-66.

100. Tang, Y.; Kong, X.; Xu, A.; Dong, B.; Lin, W., Development of a two-photon fluorescent probe for imaging of endogenous formaldehyde in living tissues. *Angewandte Chemie International Edition* **2016**, *55* (10), 3356-3359.

101. Nobbmann, U., Polydispersity–what does it mean for DLS and chromatography.

Material-Talks.com, (23 October 2014) **2014**.

102. Bera, B., Nanoporous silicon prepared by vapour phase strain etch and sacrificial technique. *Int. J. Comput. Appl* **2015**, 975, 8887.

103. Danaei, M.; Dehghankhold, M.; Ataei, S.; Hasanzadeh Davarani, F.; Javanmard, R.; Dokhani, A.; Khorasani, S.; Mozafari, M., Impact of particle size and polydispersity index on the clinical applications of lipidic nanocarrier systems. *Pharmaceutics* **2018**, 10 (2), 57.

104. Worldwide, M. I., Dynamic light scattering, common terms defined. *Inform white paper. Malvern Instruments Limited* **2011**, 2011, 1-6.

105. Wondraczek, H.; Petzold-Welcke, K.; Fardim, P.; Heinze, T., Nanoparticles from conventional cellulose esters: evaluation of preparation methods. *Cellulose* **2013**, 20, 751-760.

106. Gericke, M.; Schulze, P.; Heinze, T., Nanoparticles based on hydrophobic polysaccharide derivatives—formation principles, characterization techniques, and biomedical applications. *Macromolecular Bioscience* **2020**, 20 (4), 1900415.

107. Fessi, H.; Puisieux, F.; Devissaguet, J. P.; Ammoury, N.; Benita, S., Nanocapsule formation by interfacial polymer deposition following solvent displacement. *International journal of pharmaceutics* **1989**, 55 (1), R1-R4.

108. Chang, L. W.; Lo, W.-S.; Lin, P., Trans, trans-2, 4-decadienal, a product found in cooking oil fumes, induces cell proliferation and cytokine production due to reactive oxygen species in human bronchial epithelial cells. *Toxicological sciences* **2005**, 87 (2), 337-343.

109. Wu, S.-C.; Yen, G.-C.; Sheu, F., Mutagenicity and identification of mutagenic compounds of fumes obtained from heating peanut oil. *Journal of food protection* **2001**, 64 (2), 240-245.

110. Dung, C.-H.; Wu, S.-C.; Yen, G.-C., Genotoxicity and oxidative stress of the mutagenic compounds formed in fumes of heated soybean oil, sunflower oil and lard. *Toxicology in vitro* **2006**, 20 (4), 439-447.

111. Takhar, M.; Li, Y.; Ditto, J. C.; Chan, A. W., Formation pathways of aldehydes from heated cooking oils. *Environmental Science: Processes & Impacts* **2023**.

112. Wu, S.-C.; Yen, G.-C., Effects of cooking oil fumes on the genotoxicity and

oxidative stress in human lung carcinoma (A-549) cells. *Toxicology in vitro* **2004**, *18* (5), 571-580.

113. Xu, H.; Lv, L.; Hu, S.; Song, D., High-performance liquid chromatographic determination of hexanal and heptanal in human blood by ultrasound-assisted headspace liquid-phase microextraction with in-drop derivatization. *Journal of Chromatography A* **2010**, *1217* (16), 2371-2375.

114. Lili, L.; Xu, H.; Song, D.; Cui, Y.; Hu, S.; Zhang, G., Analysis of volatile aldehyde biomarkers in human blood by derivatization and dispersive liquid-liquid microextraction based on solidification of floating organic droplet method by high performance liquid chromatography. *Journal of Chromatography A* **2010**, *1217* (16), 2365-2370.

115. Chen, F.; Wang, C.; Zhang, M.; Zhang, X.; Liu, Y.; Ye, J.; Chu, Q., Sensitive determination of endogenous hexanal and heptanal in urine by hollow-fiber liquid-phase microextraction prior to capillary electrophoresis with amperometric detection. *Talanta* **2014**, *119*, 83-89.

116. Song, D.; Gu, Y.; Liang, L.; Ai, Z.; Zhang, L.; Xu, H., Magnetic solid-phase extraction followed by high performance liquid chromatography for determination of hexanal and heptanal in human urine. *Analytical Methods* **2011**, *3* (6), 1418-1423.

117. Phillips, M.; Gleeson, K.; Hughes, J. M. B.; Greenberg, J.; Cataneo, R. N.; Baker, L.; McVay, W. P., Volatile organic compounds in breath as markers of lung cancer: a cross-sectional study. *The Lancet* **1999**, *353* (9168), 1930-1933.

118. Ebeler, S. E.; Clifford, A. J.; Shibamoto, T., Quantitative analysis by gas chromatography of volatile carbonyl compounds in expired air from mice and human. *Journal of Chromatography B: Biomedical Sciences and Applications* **1997**, *702* (1-2), 211-215.

119. O'Neill, H.; Gordon, S.; O'Neill, M.; Gibbons, R.; Szidon, J., A computerized classification technique for screening for the presence of breath biomarkers in lung cancer. *Clinical chemistry* **1988**, *34* (8), 1613-1618.

120. Preti, G.; Labows, J.; Kostelc, J.; Aldinger, S.; Daniele, R., Analysis of lung air from patients with bronchogenic carcinoma and controls using gas chromatography-mass spectrometry. *Journal of Chromatography B: Biomedical Sciences and*

Applications **1988**, 432, 1-11.

121. Saadati, N.; Abdullah, M. P.; Zakaria, Z.; Sany, S. B. T.; Rezayi, M.; Hassonizadeh, H., Limit of detection and limit of quantification development procedures for organochlorine pesticides analysis in water and sediment matrices. *Chemistry Central Journal* **2013**, 7, 1-10.





จุฬาลงกรณ์มหาวิทยาลัย
CHULALONGKORN UNIVERSITY

VITA

NAME Faiza Lawan Isah

DATE OF BIRTH 19 February 1992

PLACE OF BIRTH Kano Nigeria

INSTITUTIONS ATTENDED 2021 - 2023 Master's degree in Chemistry, Faculty of Science, Chulalongkorn University, Bangkok, Thailand

2014 - 2017 Bachelor's degree in Industrial Chemistry, Faculty of Science, Bayero University Kano, Nigeria

HOME ADDRESS Kawo Nassarawa LGA Kano Nigeria



จุฬาลงกรณ์มหาวิทยาลัย
CHULALONGKORN UNIVERSITY